Supporting Information for Greenhouse Gases, Climate Change, and the Transition from Coal to Low-Carbon Electricity

N P Myhrvold[1] and K Caldeira[2]
[1] Intellectual Ventures, Bellevue, WA 98005, USA
[2] Department of Global Ecology, Carnegie Institution, Stanford, California 94305, USA

Email: kcaldeira@carnegie.stanford.edu

Supporting Equations

SE 1. Mathematical Models of Power Plant Emissions

SE1.1. Power Plant Emissions

We represent the life of a power plant as two distinct phases: a construction period followed by a period of operation. Construction occurs from time 0 to time t_k^{c}. Operations occur from time t_k^{c} to time t_k^{f}. We assume that each plant emits greenhouse gases (GHGs) at a constant annual rate in each phase ($\vec{E}_k^{\mathrm{construction}}$ and $\vec{E}_{ik}^{\mathrm{operation}}$, respectively).

GHG emissions as a function of time are represented as a vector, $\vec{E}(t)$, whose components represent the mass emitted per unit time for each of the three principal gases: carbon dioxide, methane and nitrous oxide.

$$\vec{E}(t) = \begin{pmatrix} \mathrm{mass}_{\mathrm{CO_2}}(t) \\ \mathrm{mass}_{\mathrm{CH_4}}(t) \\ \mathrm{mass}_{\mathrm{N_2O}}(t) \end{pmatrix}$$

For a single plant of type k, operating until t_k^f,

$$\vec{E}_k(t) = \begin{cases} 0 & t < 0 \\ \vec{E}_k^{\mathrm{construction}} & 0 \le t \le t_k^c \\ \vec{E}_k^{\mathrm{operation}} & t_k^c \le t \le t_k^f \\ 0 & t > t_k^f \end{cases} \tag{1}$$

We use the term "plant lifetime" to denote the duration of plant operation ($= t_k^{\mathrm{f}} - t_k^{\mathrm{c}}$).

Nonstop provision of power requires periodic reconstruction of the plant. In cases in which we consider continuous production of electrical power, our simplified model assumes that every power plant is rebuilt after the end of its useful life. Reconstruction is started sufficiently before the end of power generation that there will be no interruption of power output. The successor plant has the same construction cost and GHG emissions characteristics as its predecessor.

$$\vec{E}_k^{\mathrm{continuous}}(t) = \vec{E}_k^{\mathrm{operation}}\theta(t - t_k^{\mathrm{c}}) + \sum_{j=0}^{M} \vec{E}_k^{\mathrm{construction}}\theta(t - j\, t_k^{\mathrm{f}})\theta\left(j\left(t_k^{\mathrm{f}} + t_k^{\mathrm{c}}\right) - t\right) \tag{2}$$

where M is the number of plant lifetimes in our study, and θ is the unit step function.

$$\theta(x) = \begin{cases} 0, x < 0 \\ 1, x \geq 0 \end{cases} \tag{3}$$

We examine the aggregate effect of building multiple power plants over a period of time. In a new build–out the emissions from each plant sum as follows:

$$\vec{E}_{\text{build-out}}(t) = \sum_{i=0}^{N} a_i \overrightarrow{E}_k(t-i) \tag{4}$$

where $\overrightarrow{E}_k$ is the continuous emission function from a plant of type k (i.e., equation (2), a_i is the number of plants constructed in year i, and N is the total number of years in the build-out. Emissions are assumed to be linearly proportional to total plant output.

This formulation allows us to study the change in GHG emissions that would be expected to occur if a given power technology E_0 (for example, coal) were replaced with a lower-GHG-emission (LGE) technology E_1, such as solar or wind.

$$\vec{E}_{\text{replacement}}(t) = \sum_{i=0}^{N} a_i (\theta(i-t)\vec{E}_0(t) + \vec{E}_1(t-i)) \tag{5}$$

SE1.2. Atmospheric Greenhouse Gas Concentrations

The amount of each GHG in the atmosphere at any point in time can be estimated by a convolution of the emissions over time with an impulse response function kernel that describes the atmospheric lifetime of each of the three principal GHGs.

$$\vec{m}(t) = \int_0^t \vec{E}(s) \cdot G(t-s) ds \tag{6}$$

The change in atmospheric concentration of a given greenhouse gas depends on many factors, including changes in concentrations of other GHGs and in the climate. Nevertheless, following the IPCC we approximate the change in GHG concentrations by a simple impulse response function [5, 14].

$$G_{\text{CO}_2}(t) = 0.217 + .259\, e^{-t/172.9} + .338\, e^{-t/18.51} + .186\, e^{-t/1.186} \tag{7}$$

$$G_{\text{CH}_4}(t) = e^{-t/12} \tag{8}$$

$$G_{\text{N}_2\text{O}}(t) = e^{-t/114} \tag{9}$$

where represent the concentration of CO_2, CH_4, and N_2O, respectively, at any given time t after a unit release of each of these gases in the atmosphere at time $t = 0$.

It should be noted that equations (7–9) are approximations. Studies of long term CO_2 lifetimes [15-17] indicate that between 20% and 40% of CO_2 remains active in the atmosphere on time scales of 10K to 100K years. On time scales up to 100 years, we use (7) to illustrate the fundamental behavior of the system, understanding that precise values will depend on background emission scenarios and other factors.

For example, equation (7) may not be accurate for very high atmospheric concentrations of CO_2, or in the presence of substantial climate change, because the interaction of atmospheric CO_2 with the ocean, or other reservoirs is nonlinear and depends on many factors. However, the detailed simulation studies on which (7) is based have simulated beyond 560 ppm, including instantaneous jumps from 280 ppm to 560 ppm [18, 19]. This range of both absolute concentration and change-in-concentration with time is sufficient for the ranges considered in this study.

We can use these functions to define a convolution kernel, $\vec{G}$.

$$\vec{G}(t) = \begin{pmatrix} G_{\mathrm{CO_2}}(t) & 0 & 0 \\ 0 & G_{\mathrm{CH_4}}(t) & 0 \\ 0 & 0 & G_{\mathrm{N_2O}}(t) \end{pmatrix} \tag{10}$$

Equations (1–10) were evaluated to yield the GHG concentrations in the atmosphere resulting from the deployment of a collection of power plants.

The convolutions for GHG atmospheric lifetime have analytical solutions as follows. Let $\theta(t)$ be the unit step function (3). Then the carbon dioxide in the atmosphere at time t from a constant emission occurring from time $t = 0$ to time $t = \tau$ is given by

$$\begin{aligned} mass_{CO_2}(t) = \int_0^t \theta(s)\theta(s-\tau)G_{CO_2}(t-s)ds \; = \; e^{-0.903t}\Big(-0.221e^{0.0598t} - 6.26e^{0.849t} - \\ 44.8\, e^{0.897t} + e^{0.903t}(51.3 + 0.217t) + \theta(\tau - t)\Big(0.222\, e^{0.843\tau + 0.0598t} + \\ 6.26\, e^{0.054\tau + 0.849t} + 44.8\, e^{0.00578t} + e^{0.903t}(-51.3 + 0.217\tau - 0.217t)\Big)\Big) \end{aligned} \tag{11}$$

For GHGs other than carbon dioxide, the gas in the atmosphere at time t from a constant emission occurring from time $t = 0$ to time $t = \tau$ is given by

$$\mathrm{mass_{gas}}(t) = \zeta\left(1 - e^{-\frac{t}{\zeta}}\right) + \zeta\left(-1 + e^{\frac{-t+\tau}{\zeta}}\right)\theta(t-\tau) \tag{12}$$

where ζ is the atmospheric lifetime, or 12 years for CH_4 and 114 years for N_2O.

Methane breaks down in the atmosphere owing to reactions with the hydroxl radical and ultimately forms CO_2. The resulting CO_2 then has its own atmospheric lifetime. The total CO_2 resident in the atmosphere at time t from constant annual emission of CH_4 from time $t = 0$ to time $t = \tau$ is given by

$$\mathrm{mass_{CO_2\ from\ CH_4}}(t) = \begin{cases} 583.85 + 0.290e^{-0.843t} + 206.78e^{-0.0833t} \\ -213.47e^{-0.0540t} - 577.45e^{-0.00578t} + 2.604t, & t < \tau \\ \\ 206.778\left(e^{-0.0833t} - e^{-0.0833(t-\tau)}\right) \\ +0.290\left(e^{-0.843t} - e^{-0.843(t-\tau)}\right) & t \geq \tau \\ -577.451\left(e^{-0.00578\,t} - e^{-0.00578\,(t-\tau)}\right) \\ -213.467\left(e^{-0.0540t} - e^{-0.0540\,(t-\tau)}\right) + 2.604\tau, \end{cases} \tag{13}$$

In the case of hydroelectric dams, CH_4 is produced from anaerobic decay of organic material [11, 12, 20, 21]. The absolute amount of CH_4 produced is highly dependent on site characteristics, but can be modeled by a sum of P different exponential decay times η_m, with associated carbon source masses C_m. The amount of CH_4 resident in the atmosphere is

$$\mathrm{mass_{CH_4\ from\ hydro}}(t) = \sum_{m=1}^{P} C_m \frac{12e^{-t/12}\left(1 - e^{t\left(\frac{1}{12} - \frac{1}{\eta_m}\right)}\right)\eta_m}{12 - \eta_m} \tag{14}$$

The CH_4 produced from anaerobic decay ultimately turns into CO_2, given

$$\text{mass}_{\text{CO}_2 \text{ from CH}_4 \text{ hydro}}(t) =$$

$$\sum_{m=1}^{P} C_m \left(-\frac{\eta_m}{12-\eta_m}\left(-2.604 + 17.23 + \frac{e^{-0.843t}(0.245-0.0204\eta_m)}{1.-0.843\eta_m} + \frac{e^{-0.00578t}(-3.34+0.278\eta_m)}{1.-0.00578\eta_m} + \frac{e^{-0.0540t}(-11.53+0.961\eta_m)}{1.-0.0540\eta_m} + 0.217\eta_m - \frac{0.217e^{-\frac{t}{\eta_m}}(-396.91+\eta_m)(-30.45+\eta_m)(-1.45+\eta_m)\eta_m}{(-172.9+\eta_m)(-18.51+\eta_m)(-1.19+\eta_m)} \right) \right) \tag{15}$$

In this study, hydroelectric power plants are modeled with a single exponential term $C_m = 0$ for $m \neq 1$ and $\eta_1 = 7$ by using parameters from the Glen Canyon Dam [12].

SE1.3. Radiative Forcing

To estimate the impact on climate of such emissions, however, it is preferable to look directly at the radiative forcing resulting from these elevated GHG concentrations. The effect of many power plants on GHG emissions and atmospheric concentrations may be summed, as these effects are linear and additive in our model. Radiative forcing is nonlinear in concentration, however; thus, neither ΔF nor ΔT for individual plants can simply be added to obtain the cumulative effect of a fleet of power plants. Following the IPCC, radiative forcing may be approximated by the following relations [5].

$$\Delta\text{F}_{\text{CO}_2}(m_{\text{CO}_2}) = 3.35\left(g(P_{\text{CO}_2} + \alpha\, m_{\text{CO}_2}) - g(P_{\text{CO}_2})\right) \tag{16}$$

where

$$g(p) = Log(1 + 1.2\,p + 0.005\,p^2 + 1.4 \times 10^{-6}p^3) \tag{17}$$

$$\Delta\text{F}_{\text{CH}_4}(m_{\text{CH}_4}) = 0.036\left(\sqrt{P_{\text{CH}_4} + \beta\, m_{\text{CH}_4}} - \sqrt{P_{\text{CH}_4}}\right) - f(P_{\text{CH}_4} + \beta\, m_{\text{CH}_4}, P_{\text{N}_2\text{O}}) + f(P_{\text{CH}_4}, P_{\text{N}_2\text{O}}) \tag{18}$$

$$\Delta\text{F}_{\text{N}_2\text{O}}(m_{\text{N}_2\text{O}}) = 0.12\left(\sqrt{P_{\text{N}_2\text{O}} + \gamma\, m_{\text{N}_2\text{O}}} - \sqrt{P_{\text{N}_2\text{O}}}\right) - f(P_{\text{CH}_4}, P_{\text{N}_2\text{O}} + \beta\, m_{\text{N}_2\text{O}}) + f(P_{\text{CH}_4}, P_{\text{N}_2\text{O}}) \tag{19}$$

where

$$f(M,N) = 0.47\, Log(1 + 2.01 \times 10^{-5}\,(M\,N)^{.75} + 5.31 \times 10^{-15} M(M\,N)^{1.52}) \tag{20}$$

and α, β, and γ are constants used to convert the mass of emitted gas to ppmv for CO_2 and ppbv for CH_4 and N_2O. P_{CO_2}, P_{CH_4}, and P_{N_2O} are the baseline concentrations of GHGs in the atmosphere before emissions. In this study, we use P_{CO_2}= 400 ppmv, P_{CH_4} = 1,800 ppbv, and P_{N_2O} = 320 ppbv; however, modeling was also done at P_{CO_2}= 800 ppmv and other values, which produced similar qualitative results.

$$\Delta\text{F}(m(t)) = \Delta\text{F}_{\text{CO}_2}(m_{\text{CO}_2}(t)) + \Delta\text{F}_{\text{CH}_4}(m_{\text{CH}_4}) + \Delta\text{F}_{\text{N}_2\text{O}}(m_{\text{N}_2\text{O}}) \tag{21}$$

In general, if we have two systems that in isolation produce ΔF_1 and ΔF_2, then the total we would expect if they were combined is a bit less than the sum, i.e.,

$$\Delta\text{F}_{\text{total}} < \Delta\text{F}_1 + \Delta\text{F}_2 \tag{22}$$

due to the nonlinearity of ΔF with respect to GHG concentration in (16–21) above.

SE1.4 Temperature

A large body of literature reports results from simple "slab ocean" models that estimate ΔT due to radiative forcing by increased CO_2 [6, 8, 22-24]. This literature broadly concludes that such slab ocean models are useful in developing insight, even if they lack the full capabilities of more complete air ocean coupled global circulation model (AOGCM) of the climate-ocean system.

Slab ocean models reduce to a simple one-dimensional heat equation with Neumann boundary conditions.

$$\frac{\partial \Delta \mathrm{T}}{\partial t} = k_v \frac{\partial^2 \Delta \mathrm{T}}{\partial z^2} \tag{23}$$

$$\left.\frac{\partial \Delta \mathrm{T}}{\partial z}\right|_{z=0} = \left.\frac{(\lambda \Delta \mathrm{T} - \Delta \mathrm{F}(t))}{\rho\, k_v\, f\, c_\mathrm{p}}\right|_{z=0} \tag{24}$$

$$\Delta \mathrm{T}|_{\mathrm{t}=0} = 0 \tag{25}$$

$$\left.\frac{\partial \Delta \mathrm{T}}{\partial z}\right|_{z=z_\mathrm{max}} = 0 \tag{26}$$

where f = 0.71 is the fraction of the earth covered by ocean, and ρ, c_p are the density and heat capacity of seawater. The maximum depth z_{max} is chosen as 4,000 meters. This equation leaves two free parameters: the ocean vertical thermal diffusivity, k_v, and the feedback parameter λ.

Many choices for each of these have been advanced in the literature. In one of the earliest climate modeling studies, Hansen [8] concludes that $k_v = 10^{-4}$ m^2 sec^{-1} is the best choice. Kriegler [25] does a statistical analysis of multiple AOGCM models and concludes that $k_v = 5.5 \times 10^{-5}$ m^2 sec^{-1} produces the best fit to their output.

These choices of k_v are comparable to those those of highly thermally conductive solid metals, such as copper ($k_{Cu} = 1.12 \times 10^{-4}$ m^2 sec^{-1}) or aluminum ($k_{Al} = 8.42 \times 10^{-5}$ m^2 sec^{-1}). The reason for these high values is that k_v is an effective diffusivity of mixing due to eddy diffusion. Vertical transport of heat from these eddies creates an effective diffusivity comparable with that of a highly conductive solid metal.

Many choices are also available in the literature for the feedback parameter λ [23, 25]. We use λ = 1.25 W m^2 K^{-1}, following the review by Murphy [7].

One way to understand the choice of λ is to relate it to the climate sensitivity to doubled CO_2 level $\Delta T_{2\times}$.

$$\lambda \Delta \mathrm{T}_{2\times} = \Delta \mathrm{F}_{2\times} \tag{27}$$

where $\Delta F_{2\times}$ is the radiative forcing due to doubling CO_2 concentration from 280 ppm to 560 ppm.

The value of $\Delta F_{2\times}$ depends on choice of background atmospheric CO_2 concentration and choice of formulation expressing radiative forcing as a function of atmospheric CO_2 content [5]. Here we use (16) and (17) for radiative forcing from CO_2, which yields $\Delta F_{2\times}$ = 3.97 W m^{-2}, corresponding to $\Delta T_{2\times}$ = 3.18 °C. Note that $\Delta T_{2\times}$ is the asymptotic value for ΔT over long time scales, but the time lag due to heat capacity of the slab ocean will keep $\Delta T < \Delta T_{2\times}$ for finite times.

SE2. GHG Emission Figures of Merit

In comparing the impact of power plant GHG emissions on the climate, it is useful to compare approximate figures of merit that capture some of the salient dynamics. A commonly used approach is global warming potential (GWP) [26, 27], which is used to compare the impact of different radiatively active substances by integrating their radiative forcing over a time period, typically 20 or 100 years. GWP represents the integral of

radiative forcing over some time period relative to the integrated radiative forcing of an emission of an equivalent mass of carbon dioxide:

$$GWP_\tau = \frac{\int_0^\tau \Delta\mathrm{F}_{\mathrm{gas}}(m_{\mathrm{gas}}(t))dt}{\int_0^\tau \Delta\mathrm{F}_{\mathrm{CO_2}}(m_{\mathrm{CO_2}}(t))dt} \tag{28}$$

A common approach in life-cycle assessment (LCA) is to compute the GHG emissions over a period of time, and then to convert non-CO_2 emissions to GWP. An analogous figure of merit for evaluating an LGE energy replacement build-out is given by the ratio of atmospheric-lifetime-integrated energy per unit area when using the original power plant technology versus when using whatever plant replaces it.

$$\mathrm{X}(t) = \frac{\int_0^t \Delta\mathrm{F}(\int_0^u E_{\mathrm{replacement}}(s)G(u-s)ds)du}{\int_0^t \Delta\mathrm{F}(\int_0^u E_0(s)G(u-s)ds)du} \tag{29}$$

When this ratio is greater than unity, the replacement technology is depositing more energy via radiative forcing into the climate system than the technology it is replacing. When the ratio is less than one, the replacement is depositing less energy. The crossover point between the two approaches occurs when $\mathrm{X}(t_{\mathrm{EBE}}) = 1$, where t_{EBE} is the time for energy break-even between the two technologies.

Another figure of merit based on temperature can be obtained by looking at the temperature balance in the environment.

$$\Psi(t) = \int_0^t \left(\Delta\mathrm{T}_{\mathrm{original}}(0,t) - \Delta\mathrm{T}_{\mathrm{replacement}}(0,t)\right) du \tag{30}$$

$$\Psi(t_{\mathrm{TBE}}) = 0$$

The temperature break-even time, t_{TBE}, is the point at which the cumulative temperature impact of the replacement technology on the climate has reached break-even with the original.

Economists use the internal rate of return or IRR as a figure of merit for cash-flow streams that typically have both negative (investment) and positive (returns) components over time. We can define the analogous temperature IRR or TIRR as the rate R that is the solution to the equation

$$0 = \int_0^{t_{\max}} e^{-Rt}\left(\Delta\mathrm{T}_{\mathrm{original}}(0,t) - \Delta\mathrm{T}_{\mathrm{replacement}}(0,t)\right) dt \tag{31}$$

$t_{\max} \geq t_{\mathrm{TBE}}$, with $R = 0$ when $t_{\max} = t_{\mathrm{TBE}}$ or if $\Psi(t) < 0$

Alternatively we can use (31) to calculate the $t_{\max}$ required to reach a given TIRR threshold.

The value of TIRR as a figure of merit is that it measures how much future temperature benefit, relative to the replacement, is obtained for an initial "investment" of increased ΔT caused by construction. Radiative forcing IRR, or RFIRR, can be similarly defined by replacing ΔT with ΔF.

Supporting Notes

SN1. Waste Heat and Thermal Emissions

Conventional LCA analysis tracks GHG emissions, but power plants also generate waste heat in converting energy from thermal to electrical energy, and the electricity they generate is also largely dissipated as waste heat. Waste heat from power plants is another form of forcing on the climate system. These anthropogenic heat sources generally have been dismissed as small compared with radiative forcing due to GHGs [28], but others have shown anthropogenic heat could be a substantial contributor to climate change [29, 30], and to local or regional climate effects [31, 32]. Over the long lifetime of CO_2 in the atmosphere, waste heat from, say, coal combustion is small relative to the cumulative radiative forcing from the CO_2 produced by that combustion; however, waste heat may be important for the short-term transient effects studied here.

A complete LCA accounting of waste heat in construction that includes material sourcing and construction is beyond our scope and must await new LCA studies. Here we estimate waste heat during production.

Neither the use of electricity from wind and hydroelectric plants nor the waste heat in bearings and electrical resistance contribute to additional heating of the environment because the energy they capture would otherwise wind up as heat in any case through natural dissipative processes. In contrast, all of the heat generated by (both electrical and waste) energy from coal, oil, gas and nuclear plants contributes to the heating of the environment, either at the site of electricity use or at the site of its generation.

Fossil fuel or nuclear plants with a thermal efficiency of γ on an output of P watts have waste heat in watts of $P\left(\frac{1}{\gamma}-\varepsilon\right)F_L$, where ε is the fraction of electrical energy not radiated as heat, and F_L is the coefficient of atmospheric absorption for longwave terrestrial radiation, $F_L = 0.86$. Examples of non-thermal sinks of electrical energy include stored chemical energy (e.g., reduction of aluminum oxide during aluminum production), radiation into space as radio waves or radar, or radiation as visible light, principally from nighttime outdoor lighting. The latter is likely to dominate the other two and has been estimated from satellite data [33, 34] at $\varepsilon = 0.0013$, which we use here.

Because the radiative forcing concept was defined *sensu strictu* for radiative forcing and not thermal heating, there is no commonly accepted equivalence between thermal heating and radiative forcing. The approach taken here, which takes into consideration longwave fluxes, is conservative in the sense that were longwave fluxes not considered, the importance of thermal heating would be ~16% (i.e., $1/F_L$, times) larger than calculated here.

The situation with solar photovoltaic and solar thermal power generation is essentially the same as for a fossil fuel or nuclear power plant except that we must subtract the amount of energy that the earth would have absorbed in the absence of solar power production and account for the absorption of radiation in the atmosphere. The thermal warming from these facilities is related to the change in net shortwave absorption produced by these facilities as seen from the top of the atmosphere. A solar photovoltaic (PV) or solar thermal power plant with a total output of P watts and a conversion efficiency for solar radiation of γ has a total power from the sun of P/γ incident on the collector surface.

If the collector has albedo α_c, then the energy balance is shown in Figure S1. The heat retained by the atmosphere is

$$\mathrm{H}_{\mathrm{solar}} = \frac{F_s \alpha_c P}{\gamma} + F_L(1-\alpha_c)P\left(\frac{1}{\gamma}-\varepsilon\right) \tag{32}$$

where F_s is the coefficient of absorption for shortwave radiation. The ground that the solar collector is built on has a similar expression for heat retained by the atmosphere.

$$\mathrm{H}_{\mathrm{ground}} = \frac{F_s \alpha_g P}{\gamma} + \frac{F_L(1-\alpha_g)P}{\gamma} \tag{33}$$

The difference between the two is the waste heat due to the solar collector.

$$\Delta \mathrm{H} = \frac{P}{\gamma}\,(F_L - F_\mathrm{s})\big(\,\alpha_g - \alpha_c\big) + \;\; F_L(\alpha_c - 1)P\varepsilon \tag{34}$$

If we assume that solar plants are deployed primarily in areas with little cloud cover, then reflected shortwave radiation would largely be lost to space, and F_s should be the clear-sky absorption of visible light, $F_s = 0.04$. This assumption seems valid for large-scale solar PV deployments of 100 GW_e to 1 TW_e, as studied here. Solar PV plants deployed in areas with frequent cloud cover (e.g., Germany) would potentially have a different waste heat relationship. However, such plants would also have different LCA data (due to a lower capacity factor), which is likely to be a more substantial effect.

Typical values of α_g are 0.3 to 0.5 for regions suitable for widespread solar plant deployment [35]; α_c is typically 0.05 for solar PV [36] and 0.19 for solar thermal [37].

Climate effects due to solar plant albedo have recently been considered by a related approach [36], which uses broadband absorption $F_B = 0.23$ rather than splitting out the longwave and shortwave values F_L and F_S. This approach gives a lower value for waste heat.

Solar waste heat depends on the albedo of the ground or other substrate on which the plants are installed. Solar installations on rooftops will have little to any additional waste heat due to the solar panels because α_g for roofs typically falls between 0.1 and 0.15. The roofs already have low albedo; installing solar panels does not make a substantial change in albedo. Note that the rooftops will cause anthropogenic waste heat even before the panels are installed, assuming that the ground albedo is higher than that of the rooftops.

The large-scale solar installations of 100 GW_e to 1 TW_e studied here are likely to be inappropriate for rooftop deployment, so we assume desert deployment. Figure S4 shows the fraction of waste heat for solar PV and solar thermal plants as a function of ground albedo α_g.

Waste heat from solar photovoltaics is of the same order of magnitude as that from a conventional power plant such as a coal plant, which has an effective thermal efficiency of 30%–40%.

Figure S2 shows radiative forcing from each of the three principle GHGs, as well as waste heat, as a function of time. Wind has no waste heat because wind energy would ultimately be dissipated as heat via natural processes. In the case of fossil fuel plants waste heat can be important in the first years of operation because it starts immediately, whereas radiative forcing due to GHGs builds over time.

The contribution of thermal emissions to forcing exceeds that from GHG emissions for the first ~5 months of operation for coal (figures S2C and S2D) and natural gas plants but quickly drops in relative importance and is ultimately ~1% within 40 years as radiative forcing due to GHG accumulation in the atmosphere grows. Figure S3 shows the waste heat fraction for technologies for which the detailed GHG breakdown is unavailable.

Waste heat effects may compose a substantial fraction of total climate forcing from lower-emission technologies such as solar PV, solar thermal, and nuclear (figure S3). Waste heat may account for as much 80% of climate forcing for the lowest-GHG-emission cases but <1% for the highest-emission cases. In the CCS case that has the lowest GHG emissions, waste heat is equal in its warming influence to between 14% and 70% of the warming from GHG radiative forcing.

SN2. Life-cycle Analysis (LCA) Emission Data

SN2.1 Electricity production

There is a large body of literature devoted to the LCA of electrical power plants. Life-cycle assessment results depend on many details; the figures used here are drawn from the literature and are meant to be illustrative. Particular plants or those utilizing new technologies may require different parameters.

Life-cycle assessment data is important because naive use of emissions data that does not take the entire system into account can be misleading. As an example, fossil fuel plants equipped with CCS are typically projected to capture ~90% of the emissions due to combustion directly from the flue gases. However, mining

coal, transporting it to the power plant, and manufacturing the solvents or other means of capturing the CO_2 all produce emissions [38, 39]. So would leakage of CO_2 while being transported from the power plant to the sequestration reservoir. As a result, a CCS system that captures 90% of CO_2 present in flue gases from combustion may have LCA data that shows it actually captures only about ~74% of lifetime electricity generation related GHG emissions; indeed, this is true for the CCS 1 case.

The best LCA data for our purposes would be the emitted mass of each GHG for both construction and operation phases [12]. Unfortunately, that is rare among LCA studies, which tend to use GWP (the equivalent mass of CO_2) rather than breaking out separate GHGs and which tend to lump construction and operation together and report only the total lifetime emissions. Because CH_4 and N_2O have only a small impact in most transition cases, we can use data that is limited to CO_2 equivalents with some error. Such error is smaller than the variation between published LCA studies.

Many studies of power plants report only mass of CO_2 equivalent emitted per kWh produced, averaged over the life-cycle of the plant. Unfortunately that is inadequate for our purposes, which require separate accounting for construction and operation phases. In the case of solar PV, solar thermal and wind we make the assumption that all emissions are due to construction, but in other plant types this will not suffice. It is hoped that future LCA studies will clearly distinguish between emissions associated with construction and those associated with operation. Furthermore, existing LCA studies do not include thermal emissions for the materials and construction; again we hope that future studies will provide this data.

The results of LCA analysis vary widely due to many factors, including the specific technology, its geographical location and assumptions about the energy mix in the countries of manufacture. Figure S5 shows histograms of LCA data for solar PV and wind power. Figure S6 shows radiative forcing curves for all of the LCA data collected for this study. The extreme spread in values can span two orders of magnitude. Sometimes this result is due to dramatic differences in assumptions, such as the use of natural gas to generate power for a renewable plant during periods when the renewable resource is unable to generate sufficient power.

However this is not the only source of variation, and even more assumptions, results can vary considerably. Lenzen and Wachsmann [39] studied a wind turbine design manufactured and deployed in either Germany or Brazil with either new or recycled steel. Depending on the country of manufacture, country of deployment, and use of recycled steel, they found a huge range of variation even for what was fundamentally the same design.

Even basic data inputs such as GHG emissions per kilogram of a raw material like steel or concrete vary between LCA studies; they sometimes even vary within a single study. One example is that GHG emissions due to the electricity used in the construction are often tabulated with respect to the electrical generation mix in a given country or region. Thus a solar photovoltaic cell built in Europe may have a different reported LCA cost than the identical cell built in Asia.

As a result there seems to be no definitive choice of LCA analysis. The data used here should not be interpreted as only or best values. Rather they are examples of specific values reported in the literature that give insight into general trends. In critical cases, the LCA data must be examined closely to determine the applicability to the situation of interest.

Solar and wind plant output is weather dependent. The capacity factor is defined as the ratio of average output to peak (or “nameplate”) output. It depends both on plant technology and the specific site. Typical capacity factors are 15%–20% for solar PV and 20%–40% for wind. In this study we compare plants scaled to a power plant with a 1 GW_e net output averaged over a year, which is equivalent to 8.76 TWh of total electrical energy per year; capacity factor assumptions are built into the LCA data and typically not explicitly reported.

The LCA analysis for technologies with a capacity factor that depends on the geography of deployment like solar or wind is thus dependent on assumptions about the specific deployment site.

To produce illustrative examples, the data shown in table S1 were selected. Radiative forcing for most of these cases is presented in Figure S6. As representative values, the highest and the lowest curves in each plot for Figure S6 were used in simulations. The highest-emission case is numbered 1 (e.g., Solar PV 1), and the lowest is numbered 2.

SN2.2 Electricity transmission

In many cases, population centers with high electricity demand are not located near high-quality solar and wind resources. As a result large-scale deployment plans typically call for transmission lines to be built that extend thousands of kilometers between generation facilities and large-scale electrical loads. Existing LCA studies do not cover the large-scale, long-distance transmission lines required to bring power generated from wind or solar sources to the point of consumption. An LCA estimate was compiled through industry sources for 765 kV AC transmission lines [40] and is included in table S1. Note that this includes the gross raw material quantities (steel, concrete, aluminum, copper) for both the transmission lines and the necessary substations. However this data does not include the emission cost of the manufacturing processes required to turn the raw materials into the necessary transmission lines, transformers, and other equipment.

It also does not include minor materials like the SF_6 gas used as an insulator in substation equipment. Because SF_6 is a powerful GHG with a GWP of 32,000 [5], leakage during its production, substation equipment manufacturing and ongoing substation maintenance might make a substantial contribution to the overall LCA emission analysis. This effect and others need to be quantified. The items missing from the LCA analysis would all be additive to the transmission line figures used here so they are likely to represent a conservative lower bound.

In addition to construction emissions, long-distance transmission lines also have transmission losses, which we model here as 4% of the transmitted power, including the necessary lower voltage feeder systems to accumulate power from the individual sites. We believe that the 4% number is a conservative lower bound. A more precise determination depends on how far the power is transmitted and other details that would require a true system design to evaluate.

Note that these transmission losses are only from the point of generation to the point where it enters the conventional electrical grid. Grid transmission losses amount to about 7% on average in the United States for the current grid and generation sources. These grid losses are additional to the long-distance losses and are not counted here because we are looking only at the difference between renewable energy resources and conventional power plants. Conventional power plants such as coal or natural gas plants are not strongly dependent on geographical factors, whereas renewable sources like wind and solar are unevenly distributed geographically and thus may need longer transmission networks.

The losses have two effects: they force a slightly larger build-out of the power plants themselves to yield the same net power. They also contribute directly to climate warming through waste heat. In the case of wind power the emission cost due to the larger build-out is counted, but we do not count the waste heat due to transmission losses because the wind would have otherwise dissipated the energy as heat. There is thus no extra environmental heating due to power generation from wind.

Several studies have presented conceptual designs for transmission systems that could integrate wind power [41, 42]. In the case of the United States it is estimated that 30,600 km of 765 kV AC transmission lines, as well as 89 substations, would be required for nameplate wind generation capacity of 200–400 GW_e, an amount sufficient to deliver 100 GW_e of net power [43]. We use this transmission line estimate for the Wind 1 and Wind 2 cases in this study.

In the United States, solar energy resources are more concentrated than wind resources are. Industry estimates [40] that a high-voltage transmission line system for the United States would require approximately 48,000 km of transmission lines to distribute 100 GW_e of net power output.

There are few estimates available for transmission-line requirements for build-outs of solar or wind energy at the 1 TW_e and 10 TW_e scales. Transmission line costs scale approximately linearly at the same ratio as total power. One can thus extrapolate that a 1 TW_e wind deployment will require 306,000 km of transmission lines, whereas a 10 TW_e build-out will require 3,060,000 km. These estimates are roughly consistent with other published estimates for larger-scale solar deployment [44, 45].

Note that any uncertainty in the transmission line impact is still small compared with the variation between LCA data. It is hoped that in the future better LCA studies will sharpen estimates and allow more precision.

SN3. Single power plants and power plant build-outs

SN3.1 Single plant radiative forcing and temperature

Radiative forcing ΔF and temperature ΔT for various power plant technologies are shown in figure S7 for a single plant rebuilt as needed to maintain a constant output of 1 GW_e. In the early years of transitions to natural gas and CCS, temperatures increase more than they do in the best case of continued coal-based energy production modeled here, but the temperature increases are not as high as those resulting from continued use of coal plants having the highest GHG emission rates. Figures S7C and S7D show renewable technologies, while figures S7E and S7F show LGE energy technologies; both kinds of transitions can produce ΔT higher than continued use of coal during an extended start-up period.

SN3.2 Build-out growth models

Exponential growth (i.e., a constant growth rate) is perhaps the most widely used model for economic phenomena such as building out power plants. Other models for growth include linear and logistic models. Figure S8 shows how the models differ in reaching the same goals for N= 20 and N = 70 years.

Exponential models have two growth parameters: a starting value α_o, and a growth rate. For a given choice of α_o, the growth rate and the number of years N required to reach the total output can be calculated.

In this work, we model hypothetical build-outs that start with α_o = 1 GW_e of net output capacity. This choice allows ready comparison of different technologies. We use the same α_o value for cases having S_{total} from 100 GW_e to 10 TW_e. Note, however, that if one starts with a given α_o, it takes longer to build 10 TW_e of capacity than it does to build 100 GW_e at the same growth rate. Alternatively, if the build-out time is fixed, and then growth rates must be higher to obtain larger values of S_{total}.

Note that we interpret α_o as the start of a hypothetical build-out, not as the current installed base of power plants, which varies widely across the technologies studied here. Coal and natural gas are very widely deployed, whereas some of the other technologies such as CCS are nascent and have yet to reach the commercial market. Renewable energy technologies such as wind or solar are intermediate between the two; considerable variation exists in the installed base of solar PV, wind, and solar thermal power plants.

Figure S10 shows the same power plant technology (solar PV) built out across different scales and growth models. While the shapes of the curves change and quantitative details change, the same qualitative features are found in each case. Other growth models have been considered [46]. See section SD4 below for comparison to these other models.

SN3.3 Build-out conventions

We adopt several conventions for build-out programs as modeled in this study. These conventions have been chosen to facilitate easy comparison of results from different.

Each power-plant technology transition has a construction time and an operation time. Construction times vary from two to four years. In the supplemental text, table, and figures, we adopt the convention that build-out programs start at time t = 0 and are arranged so that electricity generation always starts at the beginning of year five. (Discussion and figures in the main text use, for clarity, a different convention in which time t = 0 corresponds to the beginning of electricity production or, in the case of conservation, of reduction in electricity production.) Given that our construction times vary between two and five years, the convention used here implies that there is an initial period of time from zero to three years during which no construction occurs.

Thus, if one compares the ΔT as a function of time for two technologies—say, nuclear (with a 5 y construction time) and solar PV (with a 2 y construction time)—in a single graph (e.g., Figure S12), or if one compares two different graphs, then the times of initial electricity output line up. We call this the "aligned construction" convention. Figure S9 shows a bar chart of construction and operation times for plants aligned to start operation in year five.

One could instead adopt a "race to construct" convention in which $t = 0$ is the start of construction, in which case electricity production begins at different times for each technology. The difference between the two conventions is a shift of up to three years, depending on the technology.

As a result of our convention, the first five years have no electricity generated by the replacement technology, and thus all power is generated by burning coal. In addition there are emissions from the construction of the plants that will begin operation in year six, year seven, and later years. This result is shown graphically in Figure S9B, which follows the construction and operational intervals for the first seven years of new plants in a 40-year build-out.

We modeled build-outs of durations from 1–100 years. In our terminology, a 1 y build-out means that all of the power is supplied by plants whose construction starts in the same year. Accordingly a 20 y build-out is completed by plants started over a 20-year interval. An example is shown in Figure S9C, which shows a 20 y build-out of a technology with a 2 y construction time and a 20 y operational lifetime. The aligned construction convention means that the 20 y build-out will be completed at the beginning of year 24, when the last new plants come online. More generally for a build-out of N years, the build-out will be completed in $N + 4$ years.

Supporting Discussion

SD1. Results for Linear, Exponential and Logistic Build-Outs

Figure S10 shows the results of build-outs with exponential growth to 100 GW_e and to 1 TW_e. Figure S11 displays model results for build-outs of all eight alternative technologies considered, using both high and low emissions estimates from LCAs.

Figure S12 plots ΔT for 40-year build-outs of 1 TW_e and 50 year build-outs of 10 TW_e under exponential (figure S12D), logistic (figure S12E), and linear (figure S12F) growth models, The coal case (black dashed line) is common to all of them and is not affected by the growth model because it has a constant output. The value of ΔT for the TW_e zero-emission (conservation) case at the end of the build-out varies from ΔT = 1.2 °C for exponential growth to ΔT = 0.95 °C for logistic growth, and ΔT = 0.79 °C for linear growth. At 100 years, the differences among the growth cases are only slightly larger: ΔT = 1.1 °C in the exponential case, 0.9 °C in the logistic case, and 0.71 °C in the linear case—lower in each case at 100 years than at 40 years.

The choice of growth model thus makes a relatively small difference in the results. In all 10 TW_e cases, substantial warming occurs regardless of which technology replaces existing coal plants.

Note that all graphs assume that ΔT = 0 °C at 400 ppm CO_2, so they do not include warming from preindustrial levels to 400 ppm CO_2.

SD2. Results for Bootstrap Models

The exponential, linear and logistic models all assume that generated electricity is used to displace coal and thus lower emissions. A very different strategy is to use a low-GHG emitting technology to bootstrap itself. This strategy is particularly interesting for wind and solar PV because each of them require substantial amounts of electricity in the manufacturing of key components. A "bootstrapping" transition starts with one plant and uses its electricity to manufacture more plants to grow exponentially. No electricity is turned over to the grid and thus no coal is replaced until the build-out goal has been installed and brought online, at which point the coal is displaced all at once.

The rate at which bootstrapping can occur depends on the energy payback time: the amount of time it takes a plant to generate the energy put into it. In the case of the solar PV plant modeled here, that is 1.36 years. If we allow for plant replacement at end of life as well as new construction, bootstrapping growth to 100 GW_e of annual output could occur in 12.8 years, and 10 TW_e could occur in 17.3 years.

Note that these figures are really a lower bound on the build-out time, because they assume that all other construction either takes zero time, or can all be done in parallel with the manufacturing of the electricity-dependent components. The fastest possible bootstrap of 100 GW_e annual output is likely to be somewhere between 10 and 15 years for solar PV. For this reason we model a range of bootstrap time periods rather than picking a single value.

In the wind transition modeled, the payback time is 0.31 years, allowing growth to 100 GW_e of output in four years and to 10 TW_e in five years.

We model a range of bootstrapping growth cases and compare them with the same growth rates in a grid-connected model in which the generated power is used to offset coal emissions. Note that electrical energy only covers some aspects of the construction. Concrete, steel and site construction are difficult to provision solely by electricity. As a result bootstrap transitions have lower but still nonzero GHG emissions. Very few LCA studies explicitly break out electricity as an input. Fortunately, some do [12], so those data are used for solar PV and wind.

Unfortunately, bootstrapping models are a losing proposition when their climate impact is compared with grid-connected build-outs. The reason is simple: it is important to replace coal as soon as possible. Although the use of bootstrapped electricity lowers GHG emissions during construction, it also prevents the electricity from being used to displace coal and from lowering those emissions. Because the GHGs emitted by coal combustion linger in

the atmosphere and contribute to climate impact over a long period of time, it is more important to start avoiding the emission early. This is illustrated by figure S13, which shows that the warming resulting from a bootstrapping approach to large build-outs of wind or solar PV vacillate for decades around the amount of warming induced by grid-connected build-outs of the same duration.

That said, the emission cost of plant construction is lower with bootstrap models in the long term, so they may have an ultimate advantage. This advantage takes a very long time long to develop, however. It should be noted that in this model, the GHG emissions for grid-connected models are held constant, even though most of the electricity used for construction should be from LGE sources in the late stages of an actual grid-connected build-out. Accounting for this shift in the emissions produced by grid power generation would lower the asymptotic GHG construction emissions to be similar to those of bootstrap models. It thus appears that bootstrapping models are not winning strategies for reducing near- to medium-term climate impact.

SD3. Results for Sensitivity to Technology Improvement

One dilemma of doing long-term modeling is that we cannot anticipate technological advances that could change the situation at some point in the future. In the case of fossil-fuel technologies, there have been steady efficiency and emissions advances over the last century, but the improvements are rather modest in scope: for example, yielding less than a doubling of thermal efficiency in even the best case. Newer technologies that are less mature and have yet to be deployed on a large scale, including solar, wind and CCS, may offer opportunities for technological advances that reduce their GHG emissions.

Although we cannot anticipate what these advances may be, we can create models to determine the sensitivity of temperature and radiative forcing to assumptions regarding future technology improvements. A simple approach is to multiply the emissions for the power plants by a technology improvement factor e^{-rt}, where r is the annual rate of improvement. Because plant construction is the dominant source of emissions, we take the current emission rate at the time of plant construction—it does not change over the lifetime of the plant—but when the replacement plant is built, it uses the then-current improvement factor.

We assume that exponential improvement continues for 100 years, then stops. At r = 0%, there is no improvement at all, and we get the conventional case. A value of r = 1% yields a factor of 2.7 improvement in the emissions per unit energy generated over 100 years. Though this may seem modest, it is a greater degree of improvement than has been achieve in the last century of progress in fossil-fueled plants. For r = 10%, emissions are 22,000 times lower in year 100 than they are in the first year. Improvements of this magnitude are not impossible; they have been obtained in the semiconductor industry, which is relevant to at least some forms of LGE energy technology. This range for r is very likely to bracket future improvements, however.

Figure S14 shows the results of improvements for solar, wind, and CCS transitions in a 1 TW_e exponential build-out. In each case the gray line represents r = 0%, and the black line represents r = 10%; other values fall in between. In all cases, $\Delta T \approx 0.13$ °C at t = 40 years for any improvement rate higher than about 1%. This result is to be expected because ΔT has a very small range at t = 40 years, even across different technologies (figure S12A).

The r = 10% line closely matches the zero-emission, conservation case for figure S12A. At t = 100 years, results range from ΔT = 0.11 °C for wind (figure S14B) to ΔT = 0.12 °C for all other technologies. Evidently the factor of 22,000 improvement caused by r = 10% is sufficiently large to drive the results close to zero emissions. This result shows that there is little point to modeling improvement rates higher than 10%.

Figure S14 shows that the sensitivity of our results to technological improvement is fairly low. The lowest-GHG-emission technologies are already close to the zero-emission case (figure 2), and at best, technology improvement drives them a bit closer to that lower bound.

The primary importance of technological improvement is to make unsatisfactory technologies more competitive. Carbon capture and storage is not very competitive when current LCA data (figure S14D) are used, having ΔT = 0.27 °C at 100 years in the CCS 1 case. CCS becomes quite competitive, however, when improvements rates are 3% or higher, corresponding to an improvement by a factor of 20 over 100 years. That

comparison assumes that CCS improves while its competitors do not; a more complete analysis would project improvement rates in all technologies.

SD4. Comparison with other build-out growth models

Drury and team [45] reported on several growth models of solar PV deployment. The models are approximately linear, quadratic and exponential and are based on methods of solar PV manufacturing. The analysis covers both the economic aspects (cost of deployment and electricity) and annual emissions both from solar PV production and from saved emissions and compares them with a fossil-fuel–dominated energy generation mix based on conditions in the United States. Climate impact including GHG atmospheric lifetime, radiative forcing and temperature increase, which are the main focus of the present work, are not investigated, and as such their work is complementary to ours.

In the terminology used here, Drury and team modeled the build-out of about 160 GW_e of net electricity generation (~800 GW_e of capacity with a capacity factor of 0.2) during a 40 y period by using three growth models. One, called the "early path" model, is nearly linear in the middle of the period and has significant deviations from linearity at the start and at the finish. A second, called the "constant path," is quadratic in time. The third, called the "late path," is roughly like an exponential growth model, although it is delayed substantially at the onset. In each case the growth models have been derived from other models, such as from models of how manufacturing capacity could be scaled over time.

The Drury and team growth models are shown in figure S15 with comparisons to the exponential, linear, and logistic models, scaled appropriately to a 40 y build-out of 160 GW_e of net output. Figure S15B shows that the Drury and team growth models have a different distribution of new plant construction with time. Figure S15C shows the ΔT for solar PV when the LCA data from the Solar PV 1 case is used; figure S15D shows the results for the Solar PV 2 case, which is similar to the LCA data analyzed by Drury and team. It is evident from these results that the Drury and team growth curves, although different from those used in this paper, ultimately lead to similar results.

The average time of emission can be defined as

$$t_{ave} = \frac{\int_0^\tau t\,\rho(t)\,dt}{\int_0^\tau \rho(t)\,dt} \tag{35}$$

where $\rho(t)$ is the annual new plant output added each year, and τ is the duration of the build-out. t_{ave} is analogous to the center of mass for the growth function and is a simple measure of the growth curve distribution. It correlates well with the ordering of the results as shown in figures S15E and S15F.

It is not surprising that the linear and logistic growth models are very close in terms of ΔT because their values for t_{ave} are also close. Meanwhile, the growth models used by Drury and colleagues have a wider range of t_{ave} and thus of ΔT.

Supporting tables

Table S1. Life-cycle analysis data varies between high (case 1) and low (case 2) emissions estimates for each power-plant technology. t^c is the construction time in years. t^f is the plant lifetime in years. γ is the thermal efficiency for fossil-fueled power plants and the incident solar energy conversion efficiency for solar power plants. Note that $\gamma = 1$ for the wind, hydroelectric, and zero-emission cases. Emission data shows the kilograms of GHGs emitted for the total construction period and for annual operation at a net electric output of 1 GW_e, except for the transmission line case, which is per kilometer of transmission line, including amortized emissions from substation construction. Note that the hydroelectric cases differ in the amount of submerged carbon subject to anaerobic decay, which is 9×10^7 kg for Hydro 1 and 3×10^7 for Hydro 2. CCS: carbon capture and storage.

				Total emissions from construction (kg)			Total emissions per year from operations (kg)			
Energy technology	t^c	t^f	γ	CO_2	CH_4	N_2O	CO_2	CH_4	N_2O	**Ref**
Natural gas 1	3	30	0.4	7.62E+08	0	0	5.30E+09	0	0	[46]
Natural gas 2	4	40	0.488	7.01E+08	0	0	3.85 E+09	2.45E+07	6395	[47]
Nuclear 1	5	35	0.4	3.67E+10	0	0	6.66E+08	0	0	[48]
Nuclear 2	4	40	0.4	9.72E+08	0	0	1.62E+08	0	0	[48]
Solar PV 1	2	20	0.09	1.74E+10	5.33E+05	4.78E+05	0	0	0	[12]
Solar PV 2	2	20	0.13	2.81E+09	0	0	0	0	0	[49]
Wind 1	4	30	1	3.25E+10	0	0	0	0	0	[50]
Wind 2	4	20	1	3.50E+08	0	0	0	0	0	[50]
Solar Thermal 1	2	20	0.16	3.73E+10	0	0	0	0	0	[51]
Solar Thermal 2	2	20	0.16	1.75E+09	0	0	0	0	0	[51]
CCS 1	4	40	0.35	4.63E+09	0	0	1.75E+09	1.32E+07	7.36E+06	[52]
CCS 2	4	40	0.35	1.08E+09	0	0	1.10E+09	0	0	[52]
Hydro 1	4	100	1	7.88E+08	5.78E+04	4.51E+04	0	0	0	[12]
Hydro 2	4	100	1	7.88E+08	5.78E+04	4.51E+04	0	0	0	[12]
Conservation (zero-emission power)	4	40	1	0	0	0	0	0	0	NA
Transmission line (per km)	2	40	NA	3.70E+05	6.85	6.26	0	0	0	NA
Coal	4	40	0.4	2.02E+08	6171	9344	6.59E+09	1.21E+06	582422	[12]

Table S2. Transmission lines required to support solar and wind technologies contribute to the CO_2 emissions produced during construction of these plants. Solar build-outs with a generation capacity of 100 GW_e are assumed to require 48,000 km of transmission lines with associated substations. Wind is assumed to require 30,600 km. The life-cycle assessment data supporting these figures does not include all possible sources of emissions and thus should be considered as a lower bound. Transmission lines make a negligible contribution to GHG emissions for most transition cases. Emission contributions due to transmission lines are meaningful for only the very lowest GHG-emitting energy technologies, such as Wind 2 and Solar Thermal 2. Power losses from transmission are not included in this table. If we assume 4.0% losses between generation and the connection to the distribution grid, then these losses will add 4.17% to plant emissions because that many additional plants must be built to yield the same net amount of power.

Energy technology	**Transmission lines required (km)**	**Contribution to CO_2 emissions (percentage of total emissions)**
Solar PV 1	48,000	1.02%
Solar PV 2	48,000	5.97%
Wind 1	30,600	0.365%
Wind 2	30,600	25.4%
Solar Thermal 1	48,000	0.476%
Solar Thermal 2	48,000	9.25%

Table S3. Time to reduce the amount of GHG warming from what would have occurred from continued use of a coal-based energy system, as calculated for eight lower-GHG-emitting (LGE) energy technologies. In each case, the technological transition initially increases warming. Substantial reductions in temperatures compared to the high-GHG-emission (HGE) case are projected to appear only decades or even centuries later. Simulation results listed here correspond to cases illustrated in figure 3B, with times spanning the range resulting from using the lowest and highest estimates from life-cycle analyses of emissions (table S1). Transitions were assumed to phase in over a 40-year built-out period that replaces 1 TW_e of coal-fired electricity generation.

	Years to achieve			
LGE energy technology	**the same amount of warming as coal**	**a 25% reduction in HGE warming**	**a 50% reduction in HGE warming**	**a 75% reduction in HGE warming**
Natural gas	2	97 to > 500	> 500	> 500
CCS	1 to 7	26 to 110	52 to > 500	210 to > 500
Hydroelectric	0 to 62	48 to 74	70 to 90	170 to >500
Solar thermal	<1 to 13	21 to 38	42 to 79	82 to > 500
Nuclear	<1 to 15	22 to 37	43 to 73	87 to >500
Solar PV	1 to 7	23 to 29	43 to 53	87 to 170
Wind	<1 to 12	20 to 32	40 to 56	77 to 230
Conservation	0	20	40	76

Table S4. Time evolution of emissions and climate effects produced by replacement of 1 TW_e of coal-fired electricity generation capacity, either by conservation or by a 40-year, linear build-out of natural-gas-fired plants (using LCA parameter set 2). (a) The effects of retaining coal generation with no replacement. Annual GHG emissions from the existing coal plants listed under "GHG emitted, total" include emission from both operations and periodic reconstruction of the plants. The emitted gas accumulate in the atmosphere in amount listed under "Atmosphere Reservoirs" and produce radiative forcing (F_{GHG}), smaller amounts of which are also caused by waste heat (F_{waste}). The forcing results in a steady increase in global mean surface temperature, which grows to 0.581 K in year 200.

(b) A linear transition from coal to natural gas scenario starts off with 975 MW_e generated from coal in year 1 and 25 MW_e generated from natural gas. Each year, the amount of electricity generated by coal decreases by 25 MW_e, and the amount generated by natural gas increases by the same amount. In year 40, the build out is complete, and no more coal generation occurs. The GHG emissions producing by coal generation decline accordingly, as shown under "GHG emitted, make-up coal", while those due to natural gas generation rise ("GHG emitted, new only"). The temperature increase due to this transition is 0.002 K in year 1, which is 101% that of coal because of the GHG emissions resulting from initial plant construction, which occurs before year 1. By year 200, the temperature increase due to natural gas is $0.394\ K$, or 68% of that of coal, and by year 500 (not shown) it is 77% of coal.

(c) The result of conservation, in which 1 TW_e of generation capacity it eliminated over 40 years without replacement. In year 1, 975 MW_e is generated from coal, and 25 MW_e of coal generation is retired each year. The ratio of temperature increase declines to 50% of coal by year 40 and to 9% by year 200.

	Temperature		**Radiative forcing (w/m²)**		**Atmosphere reservoirs (kg)**			**GHG emitted, total (kg/y)**			**GHG emitted, new only (kg/y)**			**GHG emitted, make-up coal (kg/y)**		
					CO_2	CH_4	N_2O	CO_2	CH_4	N_2O	CO_2	CH_4	N_2O	CO_2	CH_4	N_2O
Year	$\frac{T}{T_{coal}}$	T (K)	F_{GHG}	F_{waste}	$\times 10^{12}$	$\times 10^{9}$	$\times 10^{8}$	$\times 10^{12}$	$\times 10^{9}$	$\times 10^{8}$	$\times 10^{12}$	$\times 10^{9}$	$\times 10^{8}$	$\times 10^{12}$	$\times 10^{9}$	$\times 10^{8}$
(a) Coal																
1	1.00	0.002	0.013	0.0049	6.60	1.21	5.82	6.60	1.21	5.82	0.00	0.00	0.00	0.00	0.00	0.00
10	1.00	0.032	0.096	0.0049	50.82	8.56	56.01	6.60	1.21	5.82	0.00	0.00	0.00	0.00	0.00	0.00
20	1.00	0.068	0.172	0.0049	91.17	12.28	107.31	6.60	1.21	5.82	0.00	0.00	0.00	0.00	0.00	0.00
40	1.00	0.138	0.296	0.0049	158.33	14.61	197.44	6.65	1.21	5.85	0.00	0.00	0.00	0.00	0.00	0.00
100	1.00	0.323	0.580	0.0049	317.91	15.14	389.62	6.60	1.21	5.82	0.00	0.00	0.00	0.00	0.00	0.00
200	1.00	0.581	0.946	0.0049	534.58	15.15	551.76	6.65	1.21	5.85	0.00	0.00	0.00	0.00	0.00	0.00
(b) Natural gas 2																
1	1.01	0.002	0.013	0.0049	6.58	1.79	5.68	6.55	1.79	5.68	0.11	0.61	0.00	6.43	1.18	5.68
10	0.99	0.031	0.095	0.0047	47.91	34.03	48.29	5.93	7.04	4.38	0.98	6.13	0.02	4.95	0.91	4.37
20	0.96	0.066	0.164	0.0045	80.74	90.05	78.68	5.24	12.87	2.94	1.94	12.26	0.03	3.30	0.61	2.91
40	0.90	0.124	0.259	0.0040	121.55	225.33	91.64	3.87	24.53	0.06	3.87	24.53	0.06	0.00	0.00	0.00
100	0.75	0.241	0.422	0.0040	207.45	306.22	57.14	3.87	24.53	0.06	3.87	24.53	0.06	0.00	0.00	0.00
200	0.68	0.394	0.633	0.0040	331.29	306.77	28.04	3.87	24.53	0.06	3.87	24.53	0.06	0.00	0.00	0.00
(c) Conservation																
1	0.98	0.002	0.012	0.0048	6.43	1.18	5.68	6.43	1.18	5.68	0.00	0.00	0.00	6.43	1.18	5.68
10	0.87	0.028	0.082	0.0037	43.42	7.24	48.20	4.95	0.91	4.37	0.00	0.00	0.00	4.95	0.91	4.37
20	0.75	0.051	0.124	0.0024	65.38	8.24	78.36	3.30	0.61	2.91	0.00	0.00	0.00	3.30	0.61	2.91
40	0.50	0.069	0.129	0.0000	68.66	3.66	90.47	0.00	0.00	0.00	0.00	0.00	0.00	0.00	0.00	0.00
100	0.19	0.060	0.091	0.0000	48.66	0.02	53.45	0.00	0.00	0.00	0.00	0.00	0.00	0.00	0.00	0.00
200	0.09	0.052	0.073	0.0000	39.30	0.00	22.23	0.00	0.00	0.00	0.00	0.00	0.00	0.00	0.00	0.00

Supporting References

[14] Joos F and Bruno M 1996 Pulse response functions are cost-efficient tools to model the link between carbon emissions, atmospheric CO_2 and global warming *Physics and Chemistry of The Earth* **21** 476

[15] Archer D 2005 Fate of fossil fuel CO_2 in geologic time *J. Geophys. Res.* **110** 1–6

[16] Archer D and Brovkin V 2008 The millennial atmospheric lifetime of anthropogenic CO_2 *Climatic Change* **90** 283–97

[17] Cao L *et al* 2009 The role of ocean transport in the uptake of anthropogenic CO_2 *Biogeosciences* **6** 375–90

[18] Joos F, Plattner G, Stocker T, Marchal O and Schmittner A 1999 Global warming and marine carbon cycle feedbacks on future atmospheric CO_2 *Science* **284** 464–7

[19] Strassmann K M, Plattner G K and Joos F 2009 CO_2 and non-CO_2 radiative forcings in climate projections for twenty-first century mitigation scenarios *Climate Dynamics* **33** 737–49

[20] Diem T 2008 *Methane dynamics in oxic and anoxic aquatic systems* (ETH Zurich)

[21] Demarty M, Bastien J and Tremblay A 2009 Carbon dioxide and methane annual emissions from two boreal reservoirs and nearby lakes in Quebec, Canada *Biogeo. Disc.* **6** 2939–63

[22] Raper S, Gregory J and Osborn T 2001 Use of an upwelling-diffusion energy balance climate model to simulate and diagnose A/OGCM results *Climate Dynamics* **17** 601–13

[23] Raper S C B, Gregory J M and Stouffer R J 2002 The role of climate sensitivity and ocean heat uptake on AOGCM transient temperature response *J. Climate* **15** 124–30

[24] Wigley T and Schlesinger M 1985 Analytical solution for the effect of increasing CO_2 on global mean temperature *Nature* **315** 649–52

[25] Kriegler E 2005 *Imprecise probability analysis for integrated assessment of climate change* (Univ. Potsdam, Germany)

[26] Lashof D A and Ahuja D R 1990 Relative contributions of greenhouse gas emissions to global warming *Nature* **344** 529–31

[27] Rodhe H 1990 A comparison of the contribution of various gases to the greenhouse effect *Science* **248** 1217

[28] Washington W M 1972 Numerical climatic-change experiments: The effect of man's production of thermal energy *J. App. Meteorology* **11** 768–72

[29] Flanner M G 2009 Integrating anthropogenic heat flux with global climate models *Geophys. Res. Lett.* **36** 1–5

[30] Chaisson E J 2008 Long-term global heating from energy usage *Eos* **89** 253–60

[31] Block A 2004 Impacts of anthropogenic heat on regional climate patterns *Geophys. Res. Lett.* **31** 2–5

[32] Inoue K and Higashino H 2009 Effects of anthropogenic heat release on regional climate and pollutants distribution estimated by the meteorology-chemistry coupled atmospheric model *7th Intl. Conf. on Urban Climate* (Yokohama)

[33] Isobe S and Hamamura S 2000 Monitoring light energy loss estimated by the DMSP satellites *Memorie della Societa Astronomia Italiana* **71** 131–8

[34] Isobe S 2001 Light energy loss and its application to estimating global energy usage *Proc. SPIE* vol 4151 (SPIE) pp 237–45

[35] Ba M B, Nicholson S E and Frouin R 2001 Satellite-derived surface radiation budget over the African continent. Part II: climatologies of the various components *J. Climate* **14** 60–76

[36] Nemet G F 2009 Net radiative forcing from widespread deployment of photovoltaics *Env. Sci. Tech.* **43** 2173–8

[37] Kalogirou S 2004 Solar thermal collectors and applications *Prog. Energy and Combustion Sci.* **30** 231–95

[38] Koornneef J, Keulen T V, Faaij A and Turkenburg W 2008 Life cycle assessment of a pulverized coal power plant with post-combustion capture, transport and storage of CO_2 , *Int. J. Greenhouse Gas Control 2* **4** 448–67

[39] Lenzen M 2004 Wind turbines in Brazil and Germany: an example of geographical variability in life-cycle assessment *Applied Energy* **77** 119–30

[40] Heyeck M, Fleeman J and Wilcox E 2009 *pers. comm.*

[41] American Electric Power 2007 Interstate transmission vision for wind integration *Electricity Today* **19** 30–7

[42] Zweibel K, Mason J and Fthenakis V 2008 A solar grand plan. *Sci. Am.* **298** 64–73

[43] U. S. Department of Energy 2008 20% Wind energy by 2030, DOE/GO-102008-2567

[44] Fthenakis V, Mason J and Zweibel K 2009 The technical, geographical, and economic feasibility for solar energy to supply the energy needs of the US *Energy Policy* **37** 387–99

[45] Drury E, Denholm P and Margolis R M 2009 The solar photovoltaics wedge: pathways for growth and potential carbon mitigation in the US *Env. Res. Lett.* **4** 1–11

[46] Hondo H 2005 Life cycle GHG emission analysis of power generation systems: Japanese case *Energy* **30** 2042–56

[47] Spath P L and Mann M K 2000 Life cycle assessment of a natural gas combined-cycle power generation system *National Renewable Energy Laboratory, NREL/TP-570-27715*

[48] Lenzen M 2008 Life cycle energy and greenhouse gas emissions of nuclear energy: a review *Energy Conversion and Management* **49** 2178–99

[49] Fthenakis V M, Kim H C and Alsema E 2008 Emissions from photovoltaic life cycles *Env. Sci. Tech.* **42** 2168–74

[50] Kubiszewski I, Cleveland C J and Endres P K 2010 Meta-analysis of net energy return for wind power systems *Renewable Energy* **35** 218–25

[51] Lechón Y, de la Rúa C and Sáez R 2008 life cycle environmental impacts of electricity production by solar thermal power plants in Spain *J. Solar Energy Eng.* **130** 021012

[52] Pehnt M and Henkel J 2009 Life cycle assessment of carbon dioxide capture and storage from lignite power plants *International J. Greenhouse Gas Control* **3** 49–66

Supporting Figures

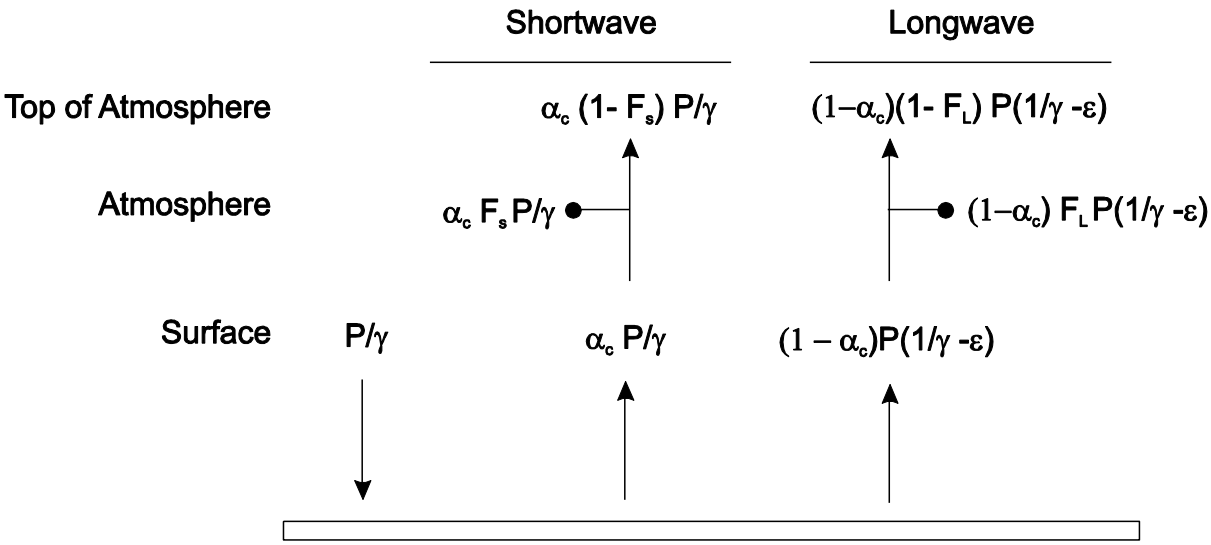

Figure S1. Energy balance is shown for a solar photovoltaic array producing P watts of power with electricity conversion efficiency γ and albedo α_c. Incident solar radiation is P/γ, and outgoing shortwave radiation is $\alpha_c P/x$. Of this, $\alpha_c F_S P/\gamma$ is absorbed by the atmosphere, and $\alpha_c(1-F_S)P/\gamma$ exits the top of the atmosphere and is lost to space. The radiation absorbed by the solar cell is $(1-\alpha_c)P/\gamma$, which is reradiated as longwave radiation, of which $(1-\alpha_c)F_L P(1/\gamma-\varepsilon)$ is absorbed by the atmosphere and $(1-\alpha_c)(1-F_L)P(1/\gamma-\varepsilon)$ exits into space. Note that absorbed radiation includes the electrical power P generated by the panel, which is assumed to ultimately be dissipated as heat except for a fraction ε. The energy balance for the ground surface before solar cell deployment is of the same form, except that albedo α_g is substituted in for α_c, and $\varepsilon = 0$.

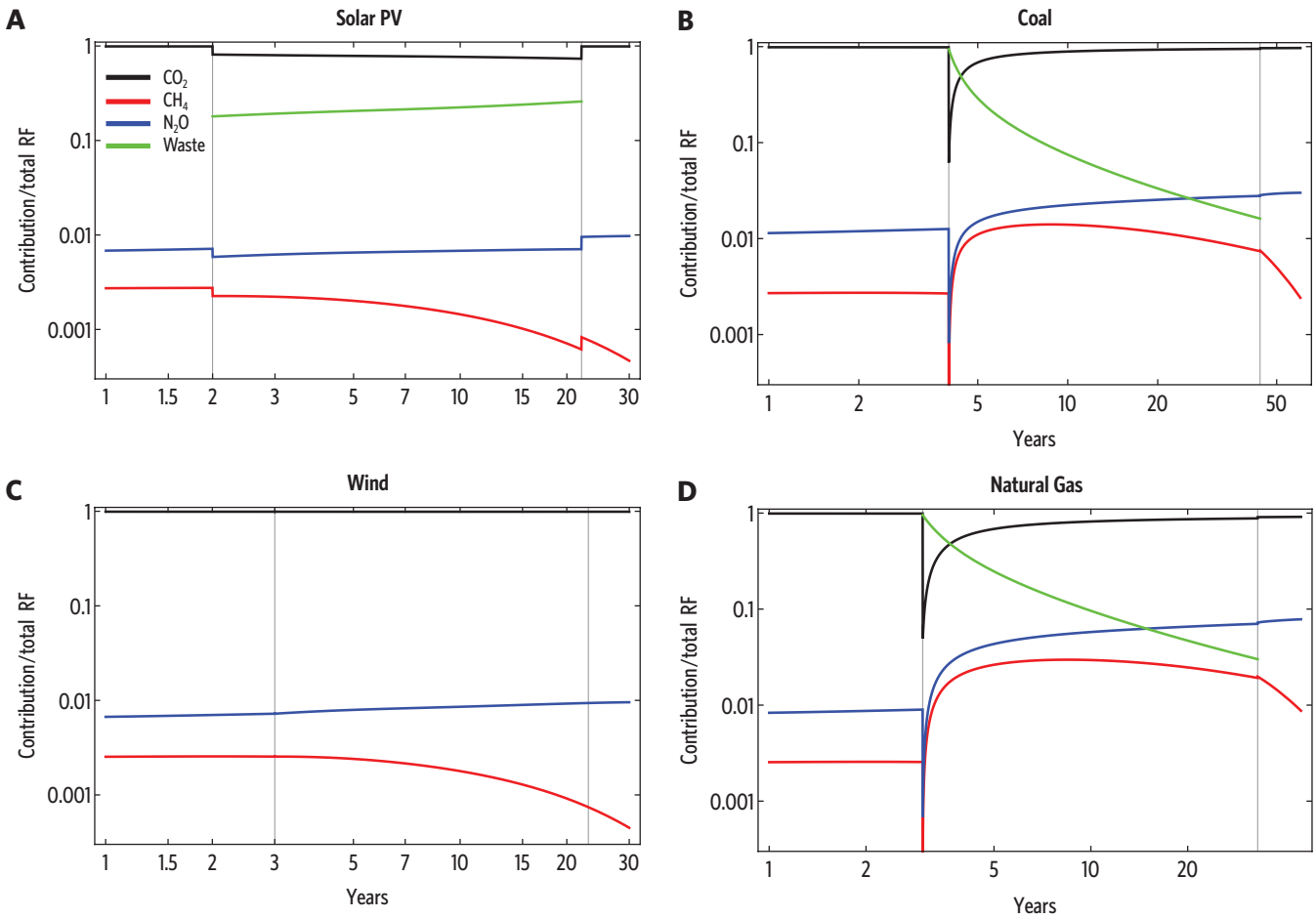

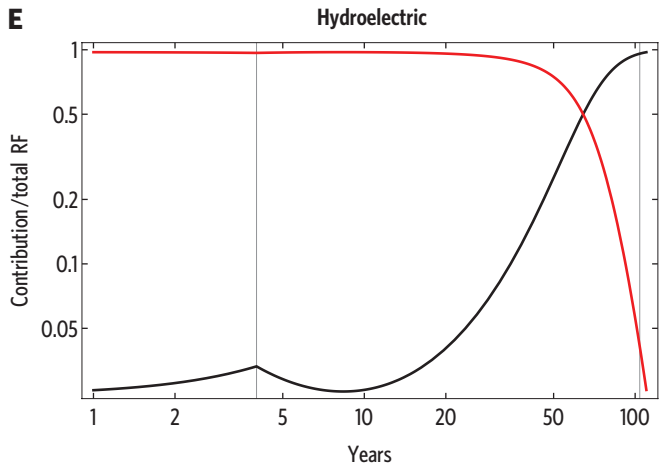

Figure S2. The relative contributions of climate forcing from various greenhouse gases (GHGs) and waste heat emissions vary among power-plant technologies, each shown here for 1 GW_e net annual output as a function of time from the start of plant construction. Vertical lines show the beginning and end of the electricity generation phase. Vertical axes represents climate forcing from greenhouse gases and waste heat as a ratio of the total radiative forcing (RF) from greenhouse gases, which may be emitted either during construction or generation. (**A**) Solar photovoltaic (PV). (**B**) Wind. (**C**) Coal. (**D**) Natural gas. (**E**) Hydroelectric. Waste heat (green lines) is emitted only during the generation phase and is assumed to be zero for wind and hydroelectric. CH_4 and N_2O are only marginally important for solar and wind, being < 1% of radiative forcing and small (< 5%) for coal and gas. CH_4 makes the dominant contribution to radiative forcing for hydroelectric. Changes in relative contribution occur primarily because of differing atmospheric lifetimes for the gases. Waste heat composes a substantial fraction of total climate forcing during the first ~5 months of coal plant operation but ultimately declines to account for <1% of climate forcing over the life cycle of the plant.

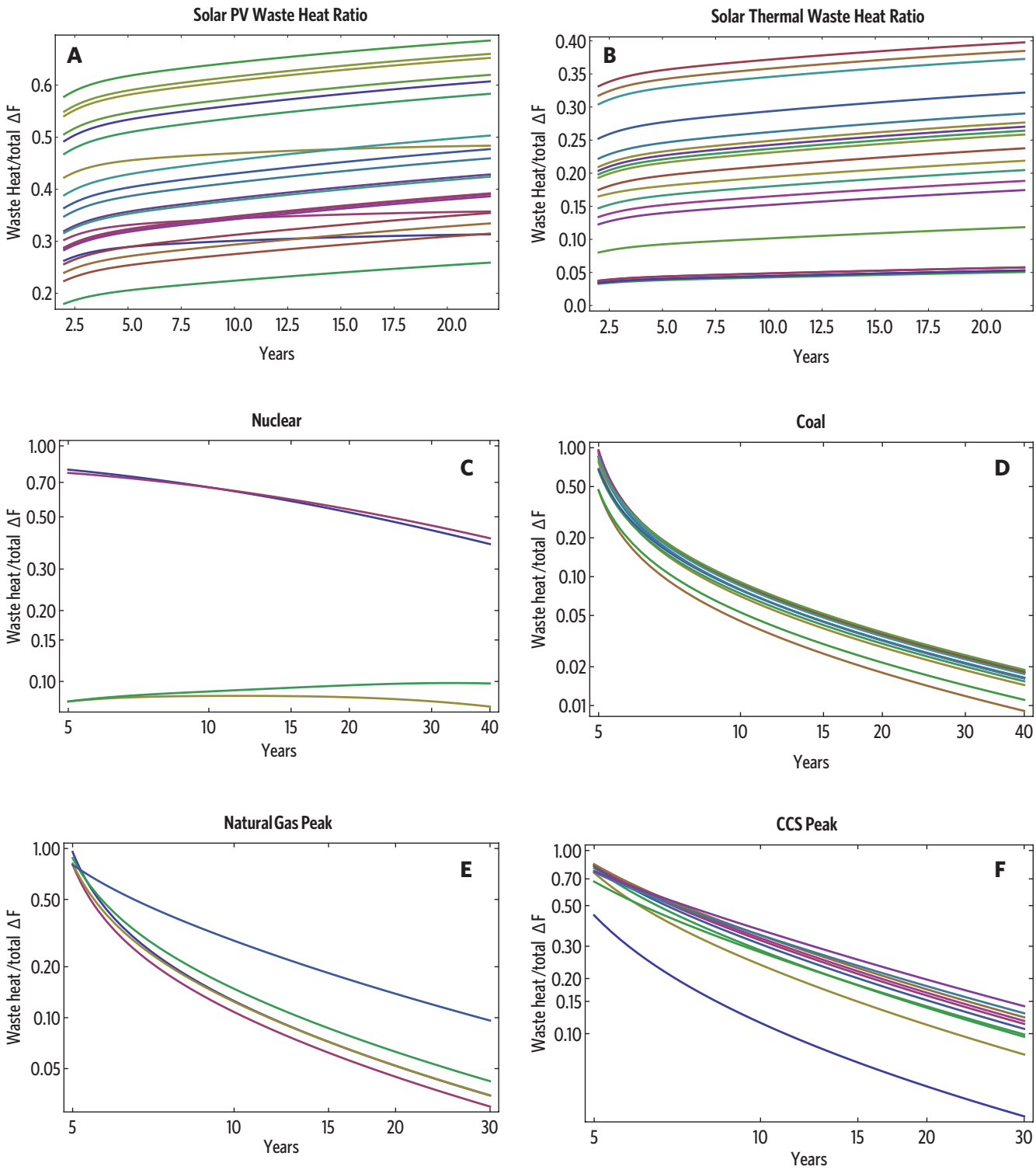

Figure S3. The ratio of waste heat to total radiative forcing changes over time and varies substantially among life-cycle assessments in the literature (each of which is shown as a separate curve). (**A**) Solar PV plants. (**B**) Solar thermal plants. Both have little variation in the ratio over time. Decay of atmospheric GHG from construction reduces total forcing, which increases the proportion due to waste heat over time. (**C**) Nuclear. (**D**) Coal. (**E**) Natural gas. (**F**) CCS.

The graph of fossil fuels curves down sharply over time as radiative forcing due to GHG emission grows linearly over time. At the start of production nearly all forcing is due to waste heat with a crossover after ~5 months for coal, but this percentage drops to 1% to 2% of the total over time. Nuclear is intermediate between solar and fossil fuel plants. The curves show relatively little variation in ratio over time. Waste heat can be substantial for low-GHG-emission energy technologies including solar, nuclear, and CCS.

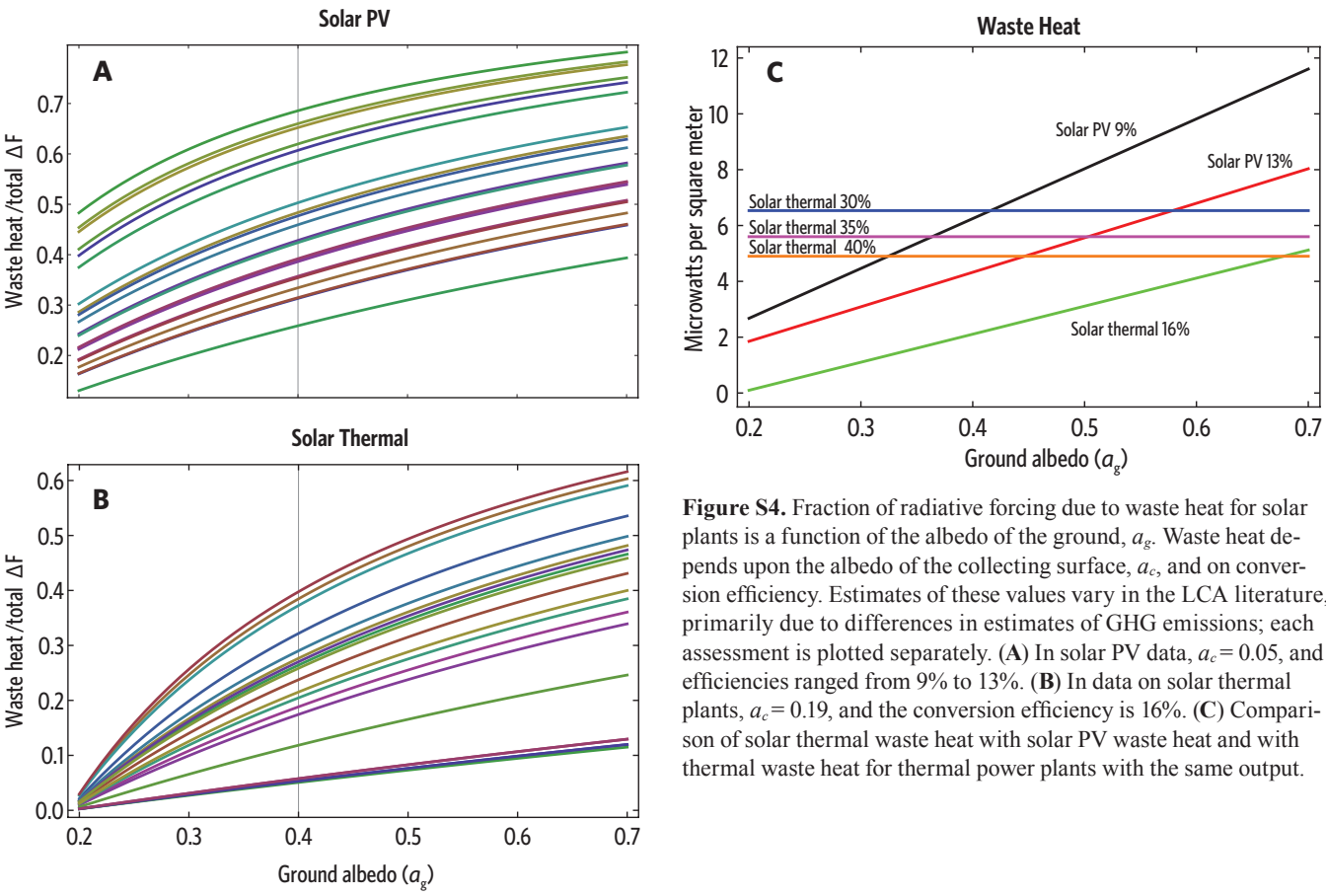

Figure S4. Fraction of radiative forcing due to waste heat for solar plants is a function of the albedo of the ground, a_g. Waste heat depends upon the albedo of the collecting surface, a_c, and on conversion efficiency. Estimates of these values vary in the LCA literature, primarily due to differences in estimates of GHG emissions; each assessment is plotted separately. (**A**) In solar PV data, $a_c = 0.05$, and efficiencies ranged from 9% to 13%. (**B**) In data on solar thermal plants, $a_c = 0.19$, and the conversion efficiency is 16%. (**C**) Comparison of solar thermal waste heat with solar PV waste heat and with thermal waste heat for thermal power plants with the same output.

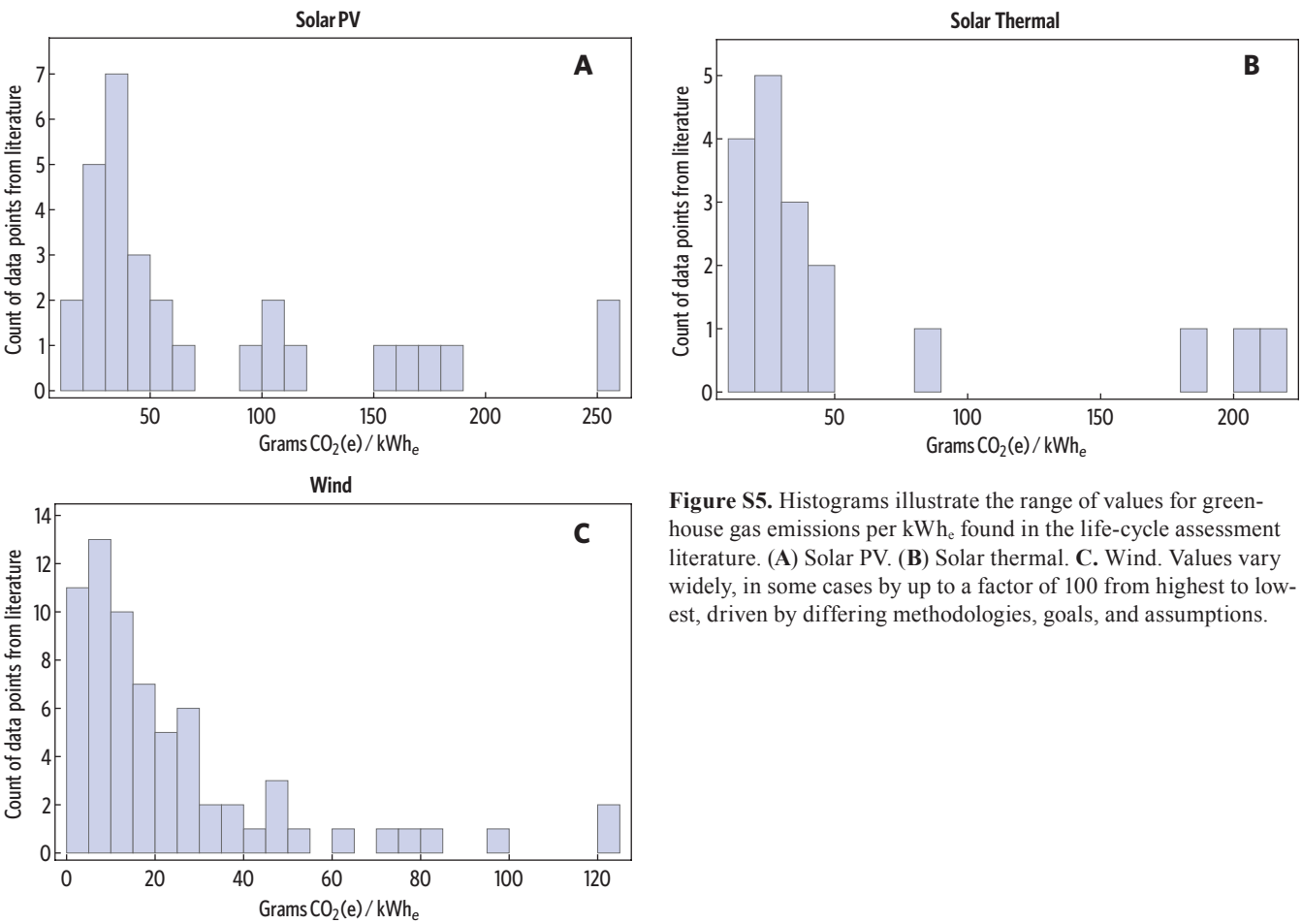

Figure S5. Histograms illustrate the range of values for greenhouse gas emissions per kWh_e found in the life-cycle assessment literature. (**A**) Solar PV. (**B**) Solar thermal. **C.** Wind. Values vary widely, in some cases by up to a factor of 100 from highest to lowest, driven by differing methodologies, goals, and assumptions.

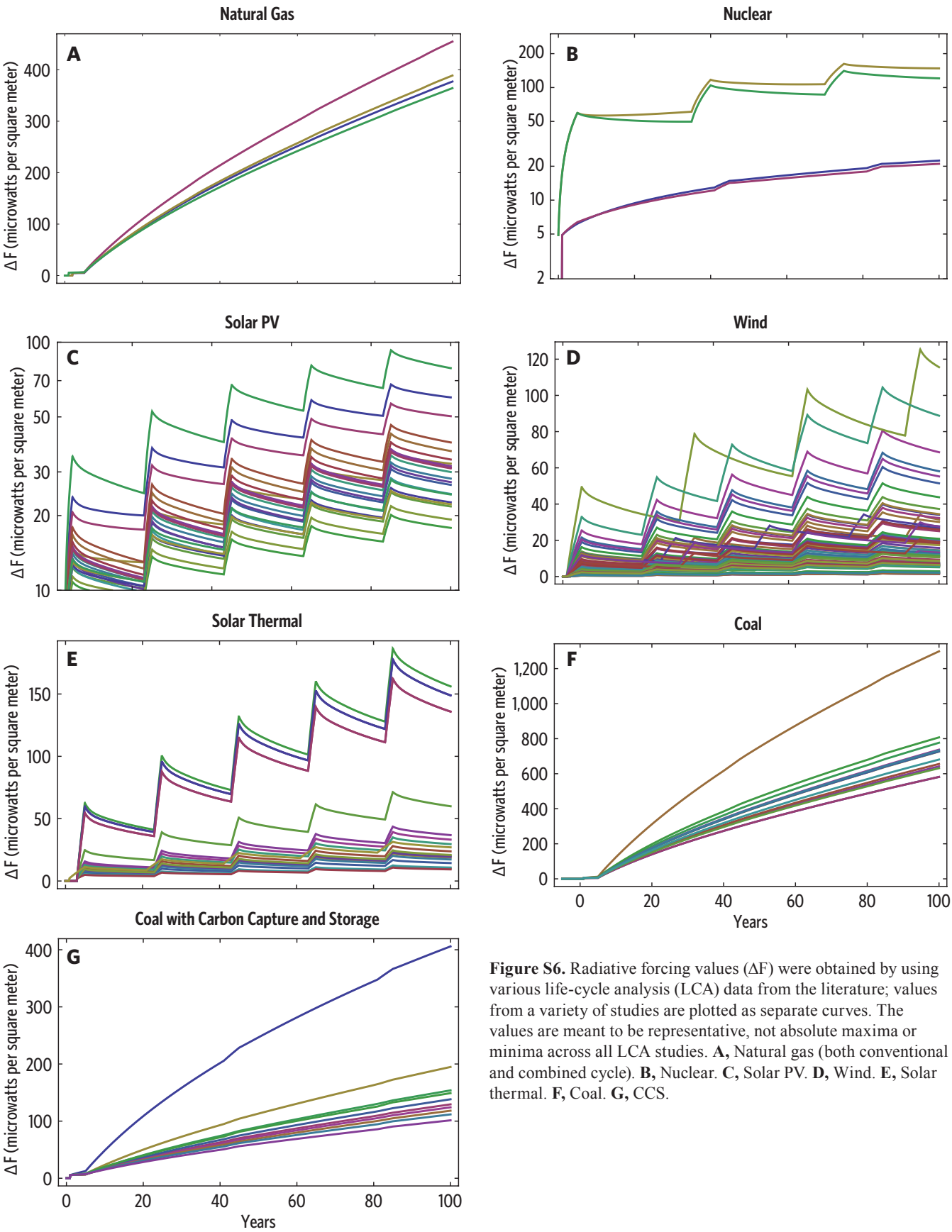

Figure S6. Radiative forcing values (ΔF) were obtained by using various life-cycle analysis (LCA) data from the literature; values from a variety of studies are plotted as separate curves. The values are meant to be representative, not absolute maxima or minima across all LCA studies. **A,** Natural gas (both conventional and combined cycle). **B,** Nuclear. **C,** Solar PV. **D,** Wind. **E,** Solar thermal. **F,** Coal. **G,** CCS.

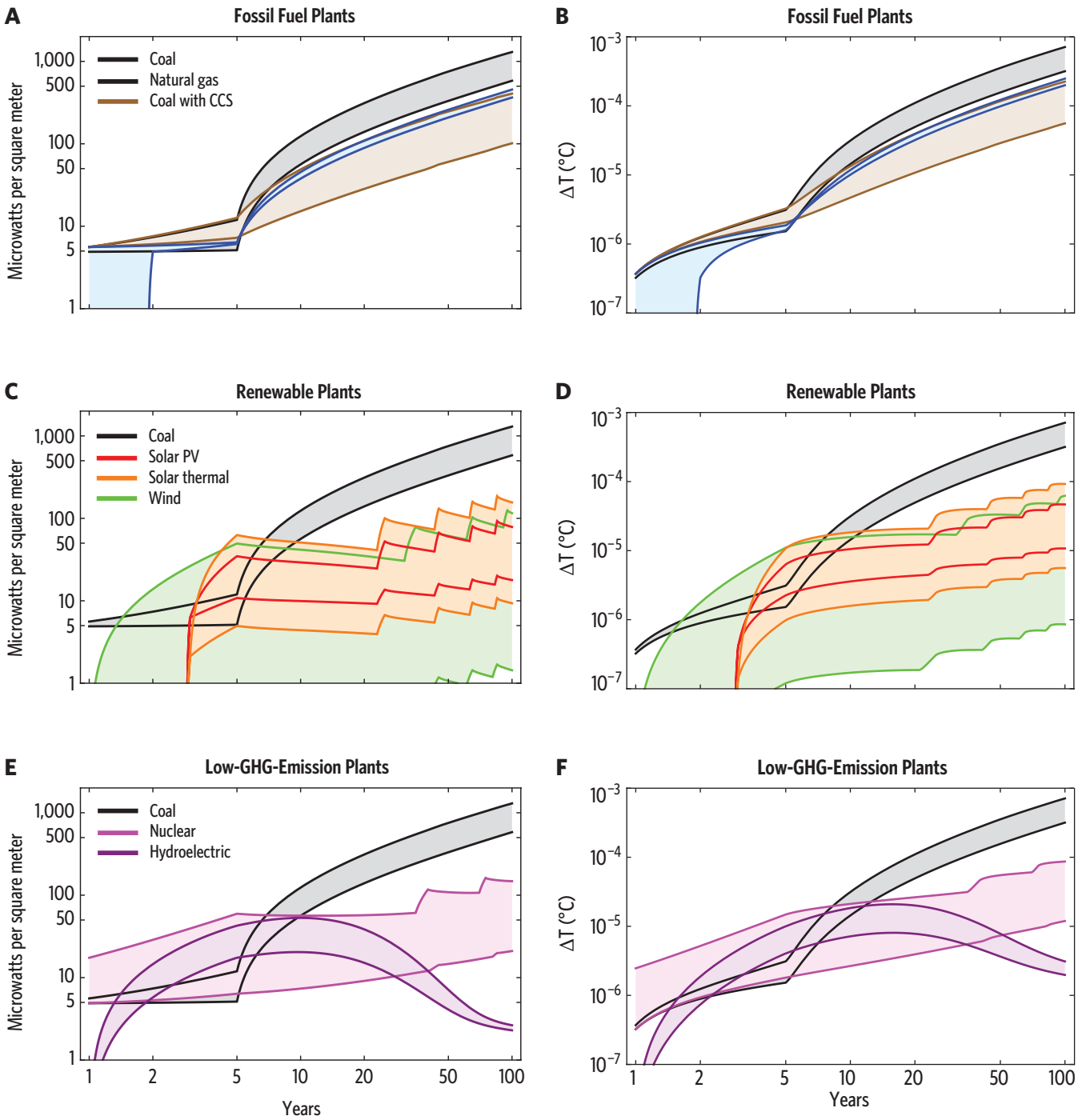

Figure S7. Radiative forcing ΔF and temperature change ΔT is shown for power plants producing a net output of 1 GW_e via different generation technologies. (**A, B**) Fossil fuel sources including coal, natural gas and CCS. (**C, D**) Renewable technologies, including solar PV, solar thermal, and wind. (**E, F**) Low-emission technologies, including nuclear and hydroelectric. Coal is shown in all plots for comparison. In each case the technologies are represented by a band bounded by typical high and low values of emissions of GHG emission values from the LCA literature.

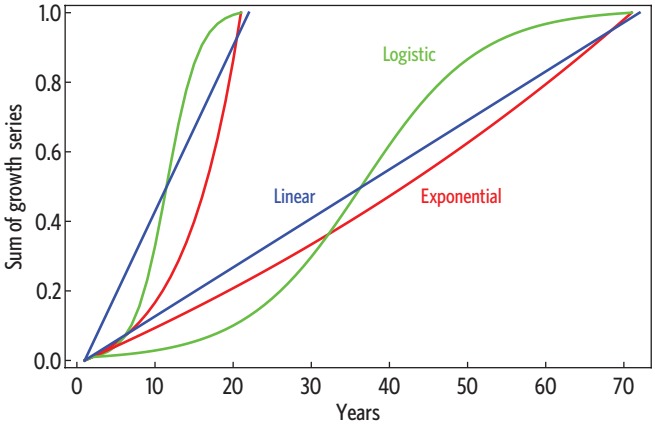

Figure S8. Exponential (red), linear (blue) and logistic (green) growth curves are shown for two power plant build-outs: one terminating in year 20 and another terminating in year 70.

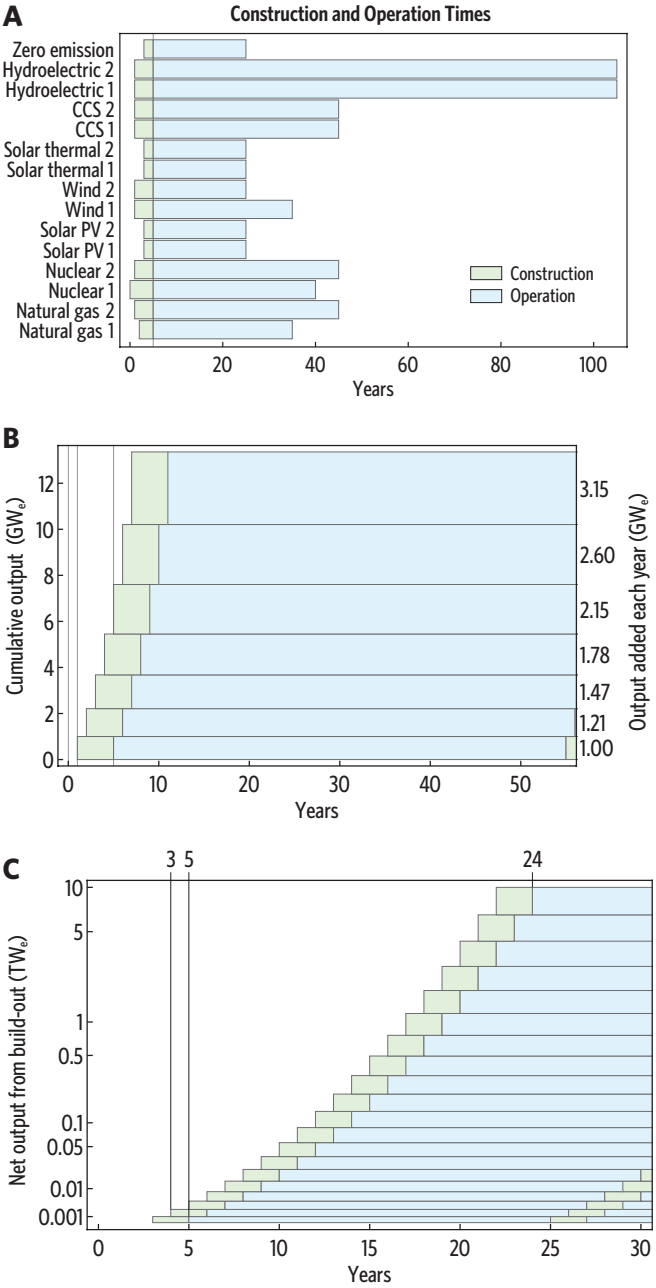

Figure S9. (**A**) Construction and operation times of power plants modeled in this paper are shown aligned so that electricity production begins in year five. (**B**) The start of plants in time (x-axis) versus net power output (y-axis) demonstraties how plant construction is staged in time. This example shows the plants on which construction started during the first seven years of new plant additions for a 10 TW_e exponential build-out; plants here are assumed to have a 4 y construction time and a 40 y operational life. In year one, construction begins on plants to produce 1 GW_e; they begin electricity generation at the beginning of year five. In year two, construction begins on plants that will produce 1.21 GW_e starting at the beginning of year six, and so forth with each addition. At the end of its 40 y operational lifetime, each plant must be reconstructed, so the cycle of construction and operation begins again. (**C**) A 20 y exponential build-out to 10 TW_e with a technology that has a 2 y construction time and a 20 y operational life. Construction begins in year three. Electricity generation begins in year five. The last new power plants to come online start production in year 24. By convention, this is a 20 y build-out because it takes 20 years of new plant starts to reach the 10 TW_e output goal.

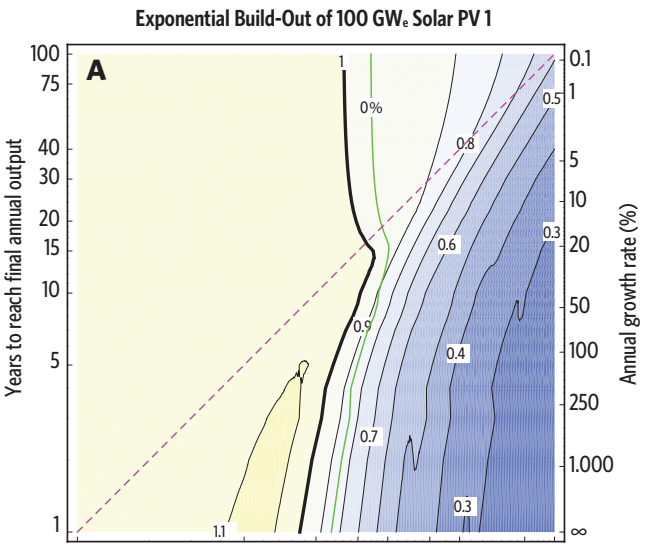

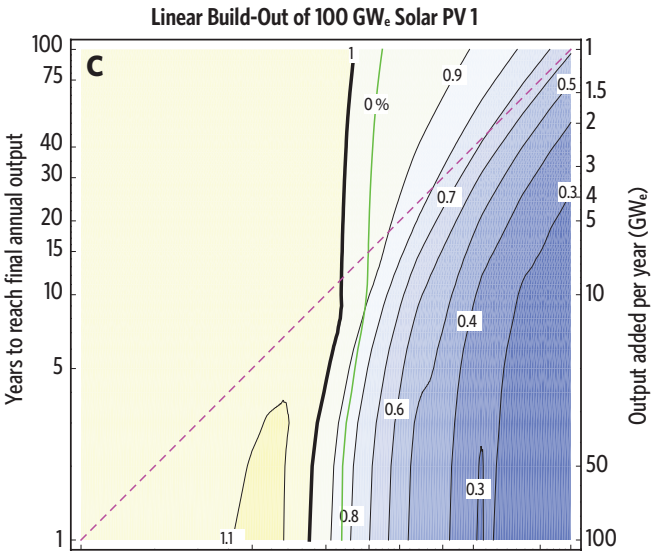

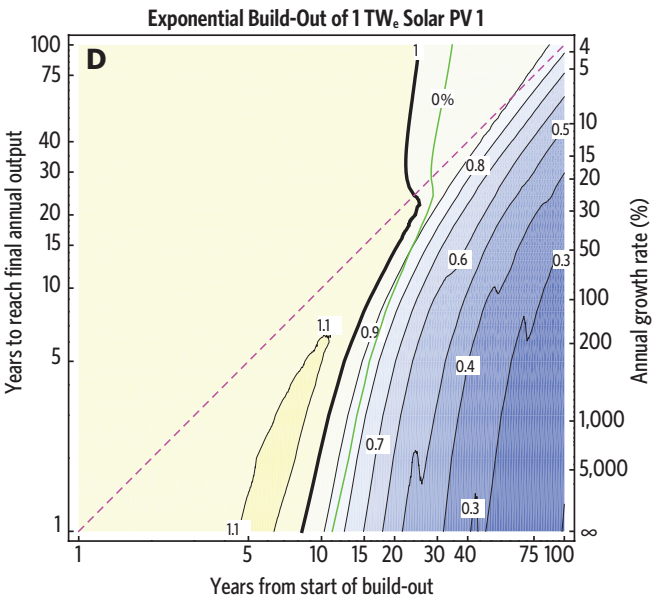

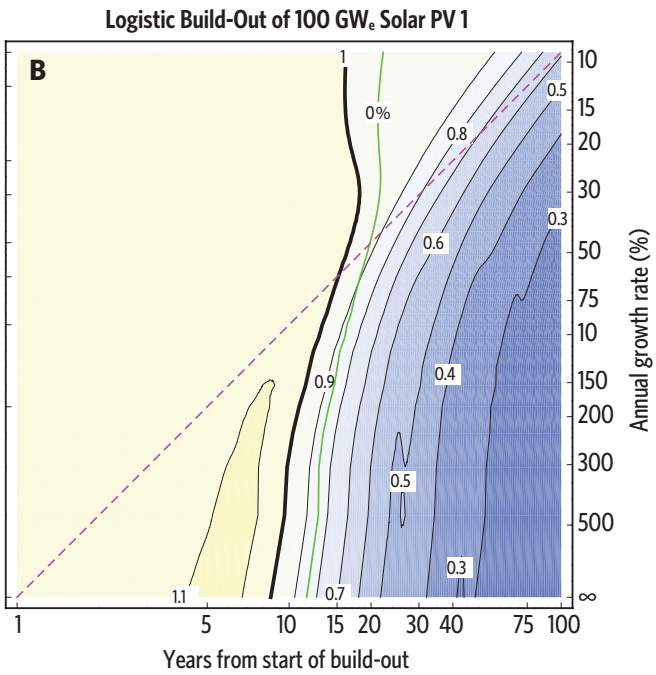

Figure S10. Build-out results for solar photovoltaic (PV) data set 1 are shown with a variety of build-out scales and growth rates. The y-axis is the speed of the build-out required to go from a 1 GW_e output to the final output level. This value can be expressed either as the number of years required to reach the final output (left axis) or the annual growth rate (for exponential growth), peak annual growth rate (for logistic growth) or annual increment (for linear growth). The x-axis is time from the start of the build-out. The dashed magenta line shows where y = x . Electricity generation starts in year five. Contour lines show the ratio of ΔT due to radiative forcing by the new plants to ΔT_{coal} that would have been produced by the coal plants displaced. The green line shows the integrated temperature break-even time, t_{TBE}. This time is equivalent to the point at which the temperature internal rate of return TIRR = 0%. All panels in this figure use life-cycle assessment data from Solar PV data set 1. (**A**) Exponential build-out to 100 GW_e. (**B**) Logistic build-out to 100 GW_e. (**C**) Linear build-out to 100 GW_e. (**D**) Exponential growth build-out to 1 TW_e. (**E, next page**) Logistic growth build-out to 1 TW_e. (**F, next page**) Linear growth build-out to 1 TW_e. If we compare graphs based on the same growth model we can see that they are qualitatively similar despite a tenfold difference in scale. All of the growth curve examples share common features, including the peak that occurs in the lower left quadrant for build-outs faster than 10–15 years.

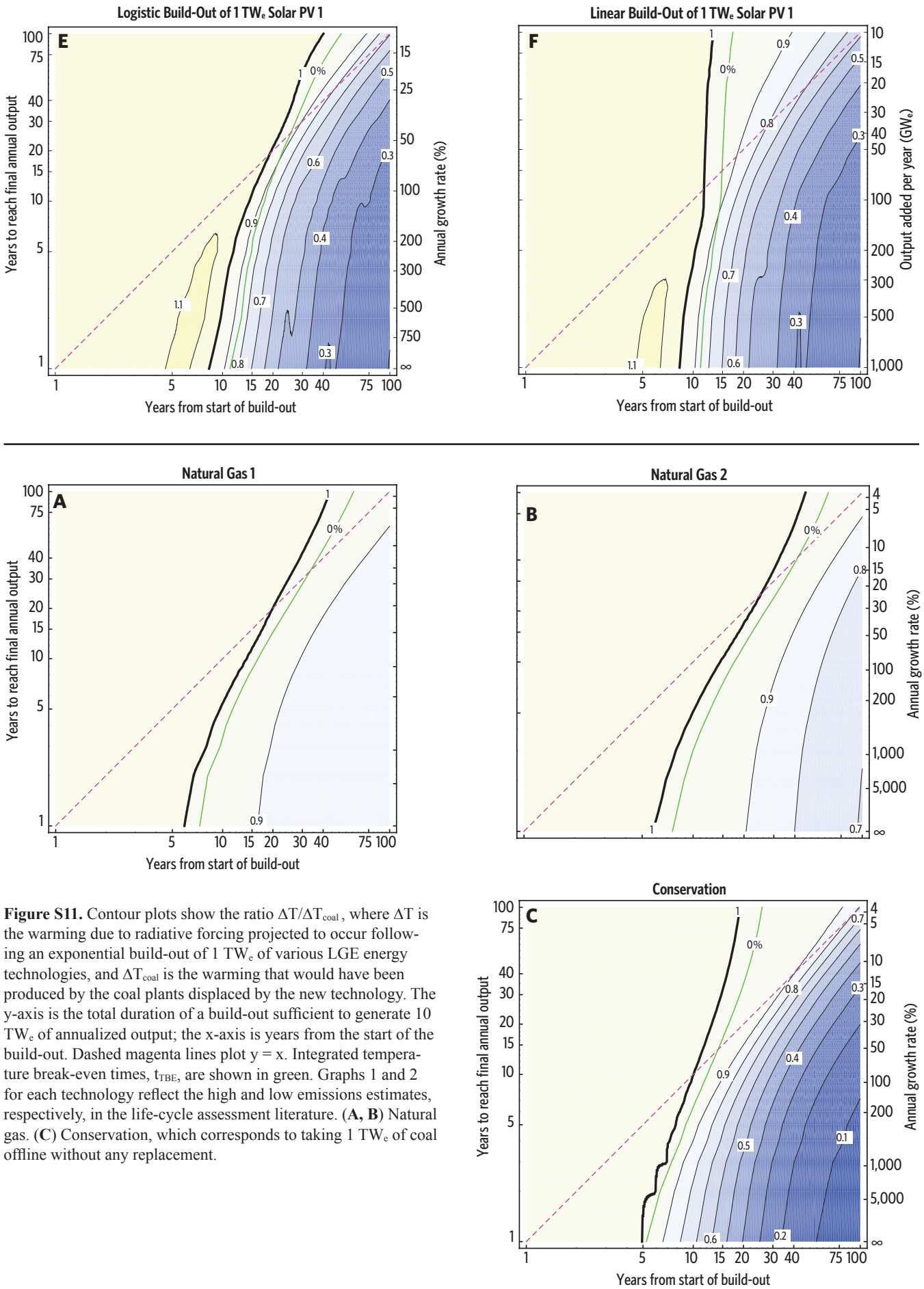

Figure S11. Contour plots show the ratio $\Delta T/\Delta T_{coal}$, where ΔT is the warming due to radiative forcing projected to occur following an exponential build-out of 1 TW_e of various LGE energy technologies, and ΔT_{coal} is the warming that would have been produced by the coal plants displaced by the new technology. The y-axis is the total duration of a build-out sufficient to generate 10 TW_e of annualized output; the x-axis is years from the start of the build-out. Dashed magenta lines plot y = x. Integrated temperature break-even times, t_{TBE}, are shown in green. Graphs 1 and 2 for each technology reflect the high and low emissions estimates, respectively, in the life-cycle assessment literature. (**A, B**) Natural gas. (**C**) Conservation, which corresponds to taking 1 TW_e of coal offline without any replacement.

Figure S11 (continued). (**D, E**) Nuclear. (**F, G**) Solar photovoltaic (PV). (**H, I**) Wind.

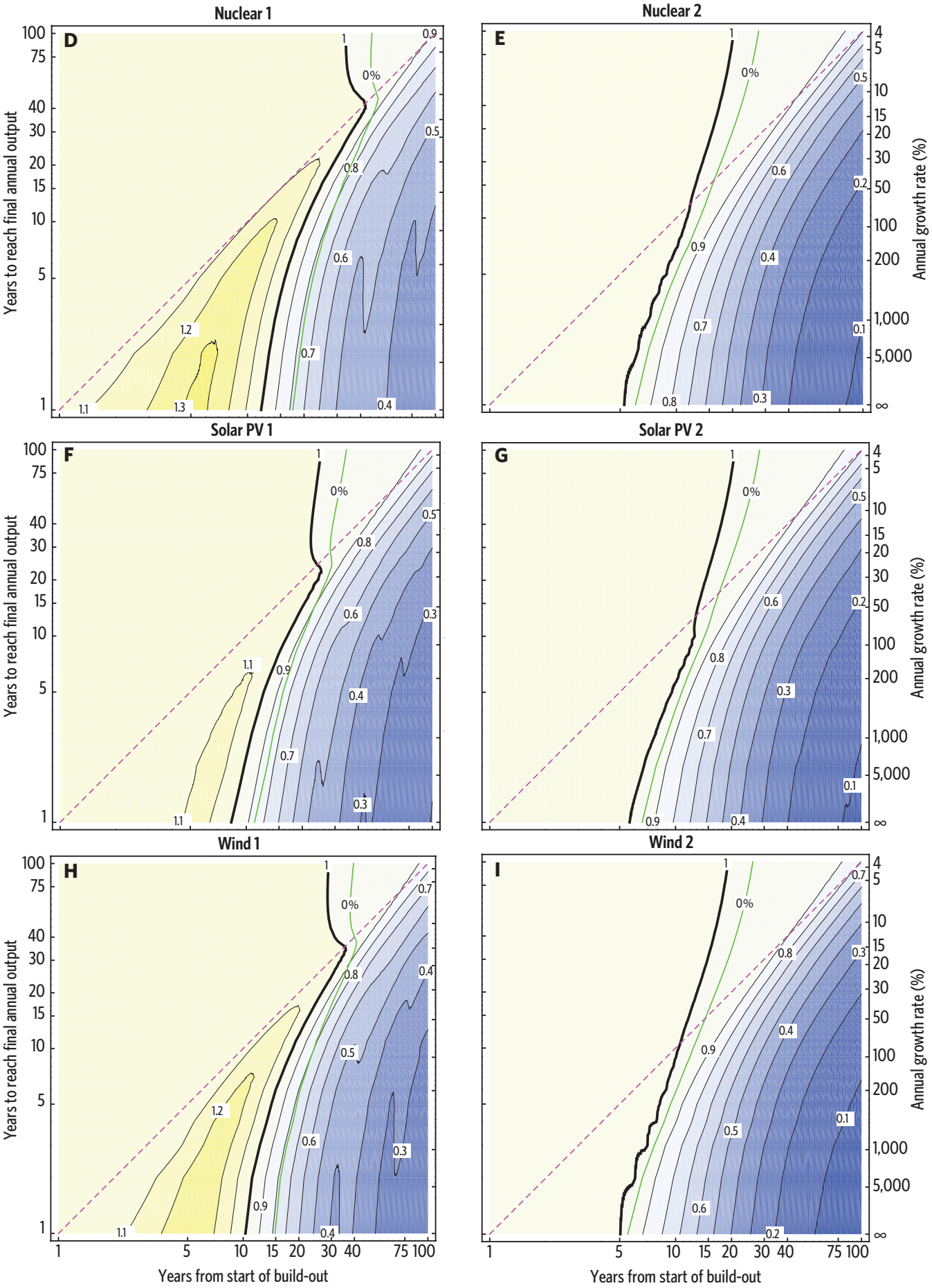

Figure S11 (continued). (J, K) Solar thermal. (L, M) Carbon capture and storage (CCS). (N, O) Hydroelectric (Hydro).

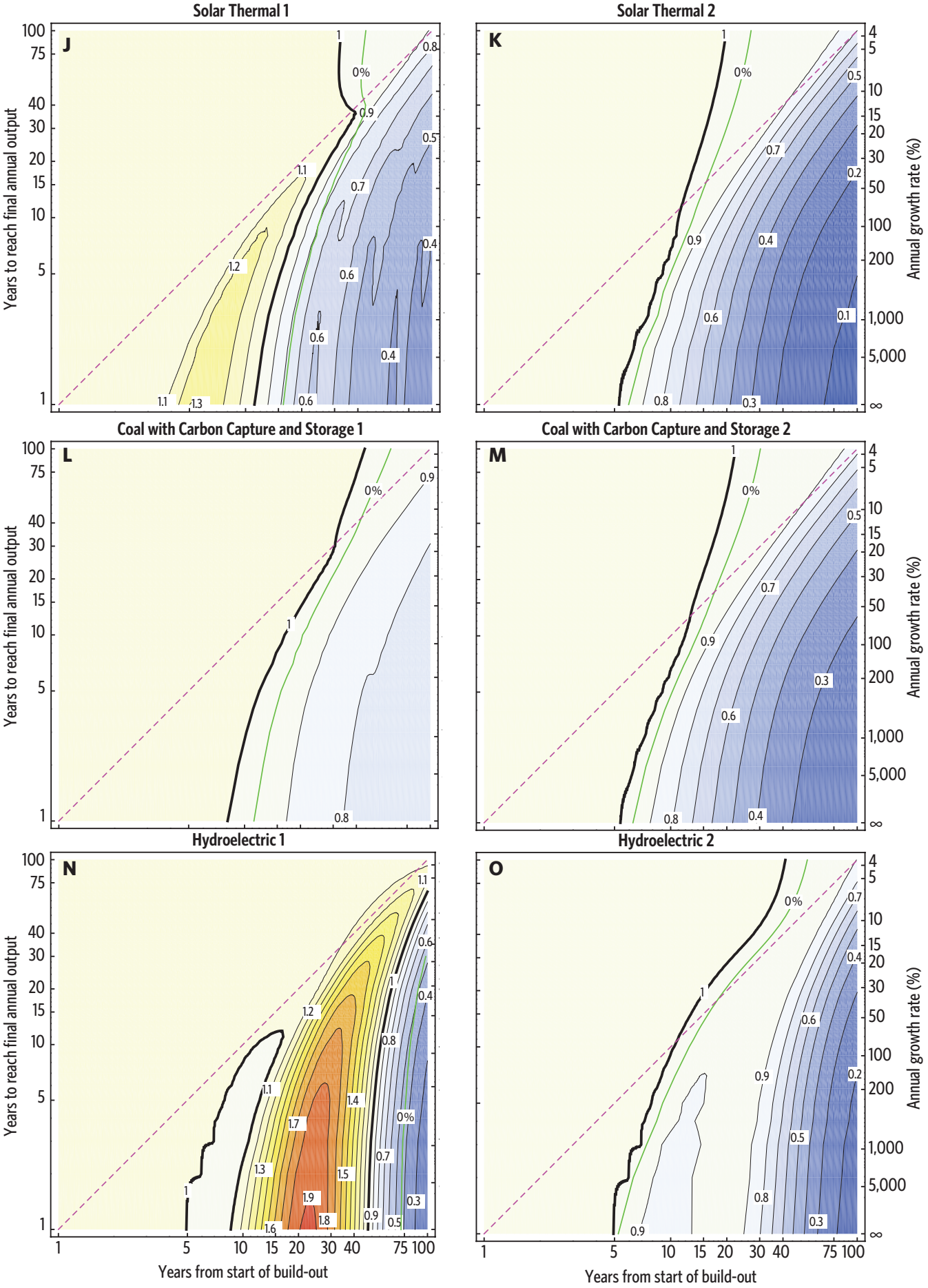

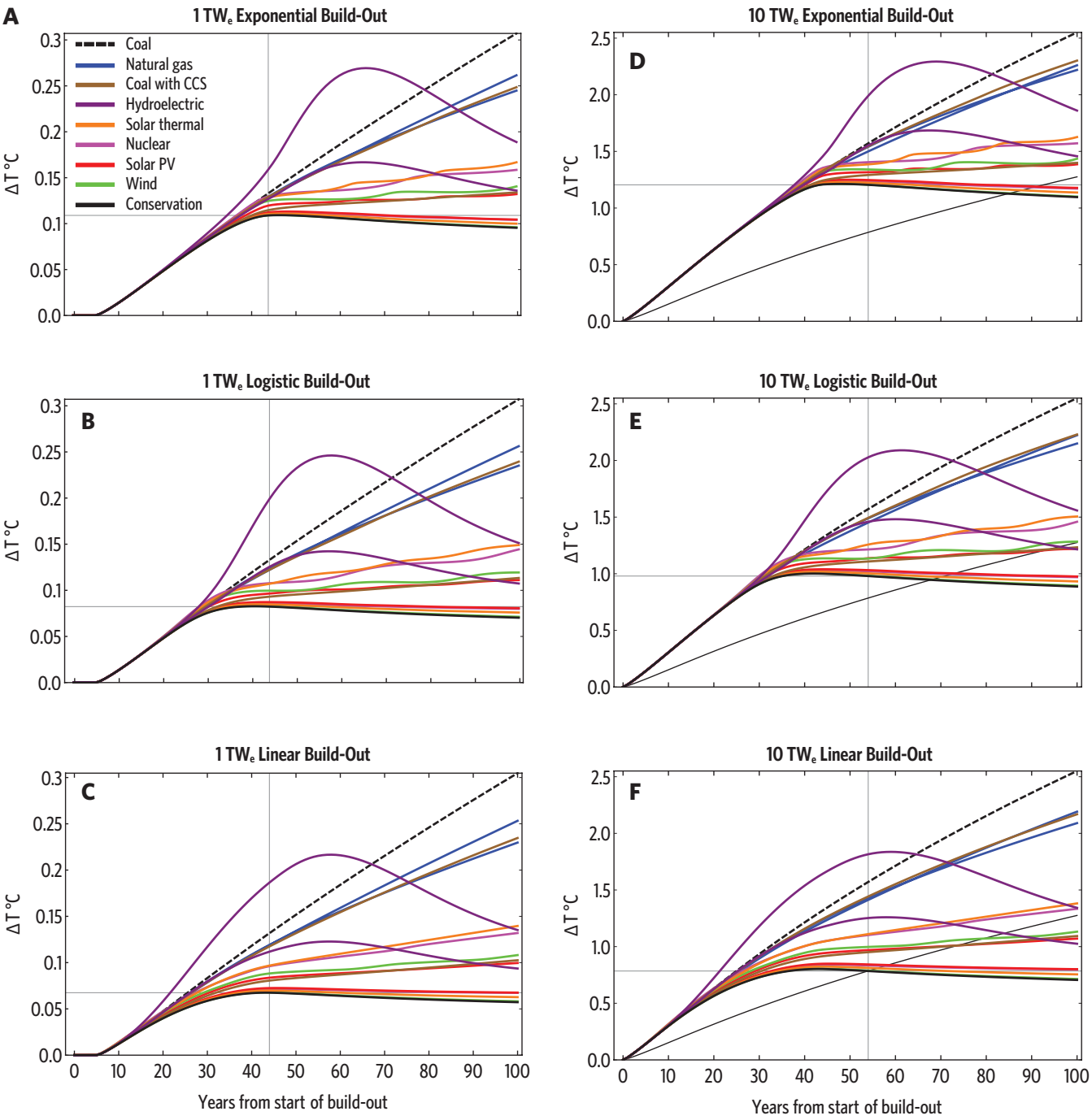

Figure S12. Temperature increase ΔT is shown for 40-year duration build-outs of 1 TW_e and 50-year build-outs of 10 TW_e of net annualized output via three different growth models. (**A**) Exponential growth to 1 TW_e starting from 1 GW_e. (**B**) Logistic growth to 1 TW_e starting from 1 GW_e. (**C**) Linear growth to 1 TW_e. (**D**) Exponential growth to 10 TW_e. (**E**) Logistic growth to 10 TW_e. (**F**) Linear growth to 10 TW_e. The vertical lines at t = 44 years and at t = 54 years mark the end of the build-outs. The horizontal lines show ΔT values for the zero-emission cases at the end of each build-out. The dashed black line shows coal, which produces 0.13 °C at 44 years and 0.32 °C at 100 years for 1 TW_e and produces 1.55 °C at 54 years and 2.55 °C at 100 years for 10 TW_e. The zero-emission case representing conservation (black line) provides a lower bound on ΔT from realistic technologies, whereas coal provides the upper bound. Sensitivity to the build-out growth curve is shown in the differences among the graphs.

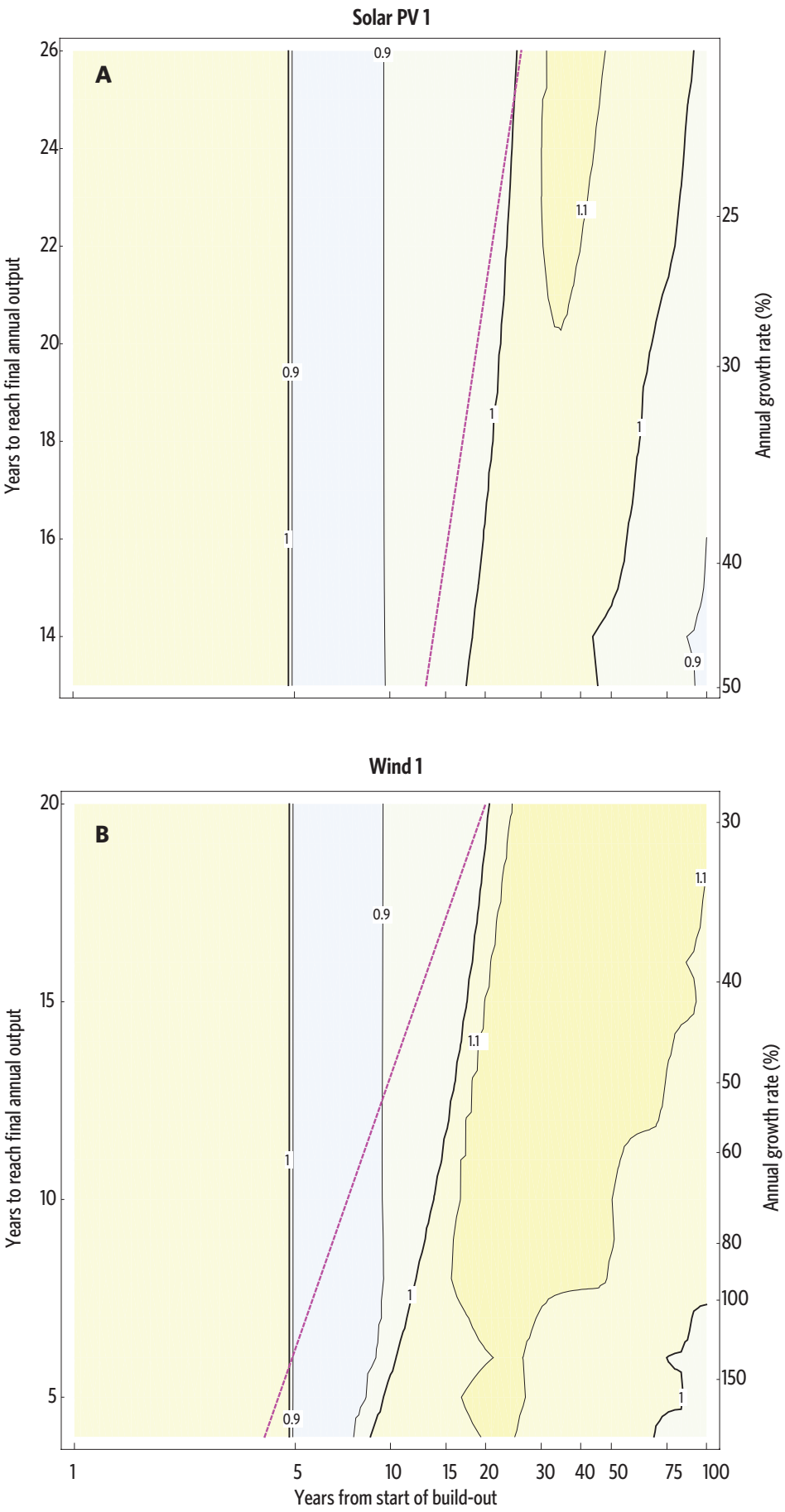

Figure S13. Results are shown for bootstrapping growth models for (**A**) solar photovoltaic (PV) and (**B**) wind transitions. Counter lines represent the ratio $\Delta T_{self}/\Delta T_{grid}$ for 1 TW_e exponential build-outs, where ΔT_{self} is the temperature increase restuling from bootstrapping growth and ΔT_{grid} is the increase from a build-out of the same technology in which power for the build-out is drawn from the grid. The dashed magenta line represents the completion of the build-out. In all cases, ΔT_{self} exceeds ΔT_{grid} for the first five years of the build-out. ΔT_{self} then dips below ΔT_{grid} for 15–20 years, after which $\iota\tau$ rises and remains above ΔT_{grid} until years 50–75 for solar PV and until at least year 70 for wind. Note that t_{TBE}, the time to temperature break-even, occurs beyond 100 years.

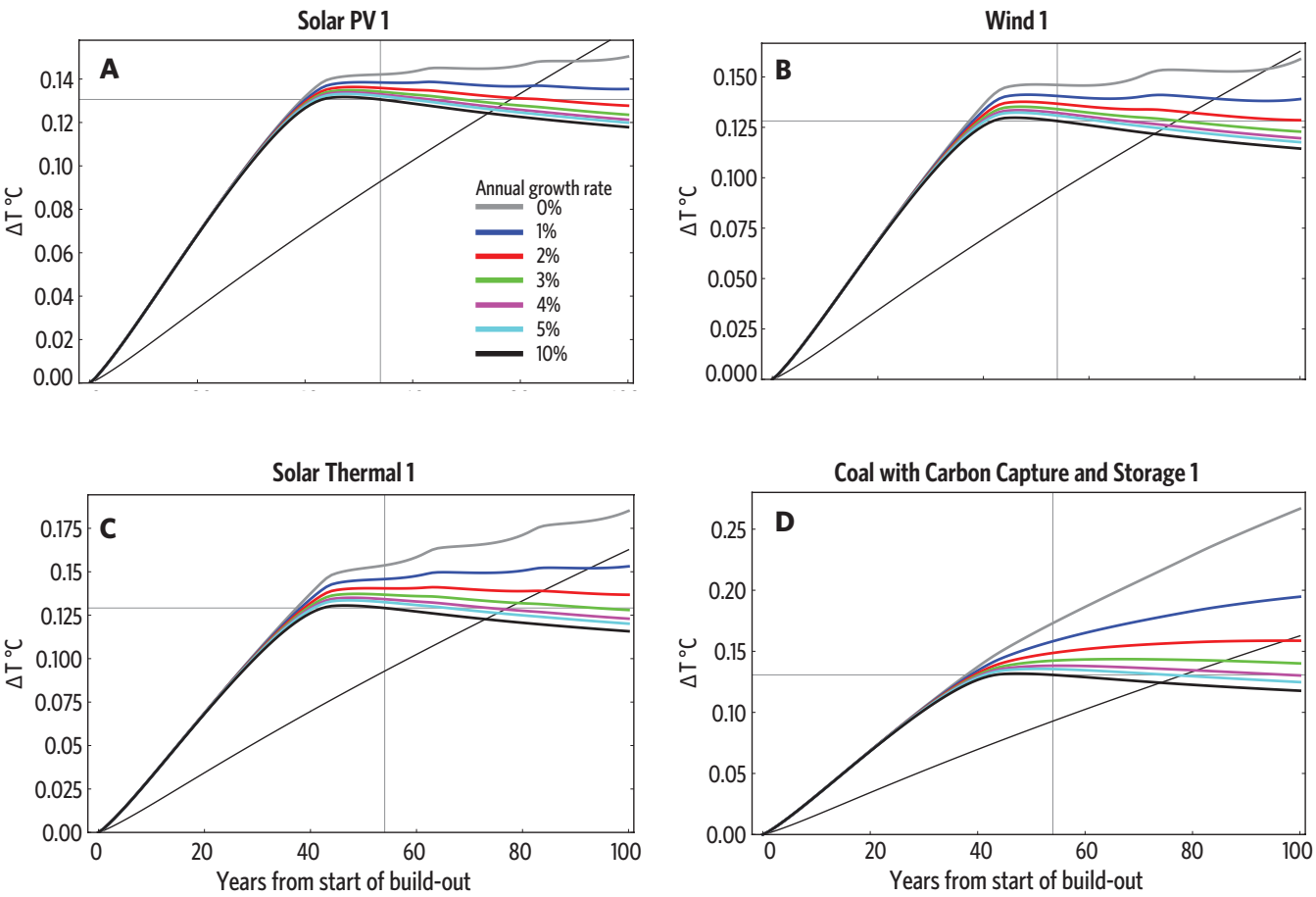

Figure S14. Temperature difference ΔT for technology improvement cases in 40-year, 1 TW_e exponential build-outs. Baseline emissions for new plants constructed are reduced by an *r*% compounded rate per annum each year for the first 100 years, and then remain constant, where *r* ranges from 0%–10%. Plants constructed in a given year use the emission profile of their construction year throughout their useful life. (**A**) Solar PV as the baseline technology. (**B**) Wind. (**C**) Solar thermal (Th). (**D**) Coal with carbon capture and storage (CCS). In each case ΔT ≈ 0.13 °C at 40 years, regardless of the value of *r*. The case with no technological improvement (*r* = 0%, gray line) is different for each technology and matches the curves for a 40 y, 1 TW_e exponential build-out. The highest improvement case (*r* = 10%, black line) is very similar for each baseline technology; ΔT ranges from 0.11 °C to −0.27 °C at 100 years. This value approximately matches the conservation (zero-emission technology) line (see other figures), which produces ΔT = 0.11 °C at 100 years.

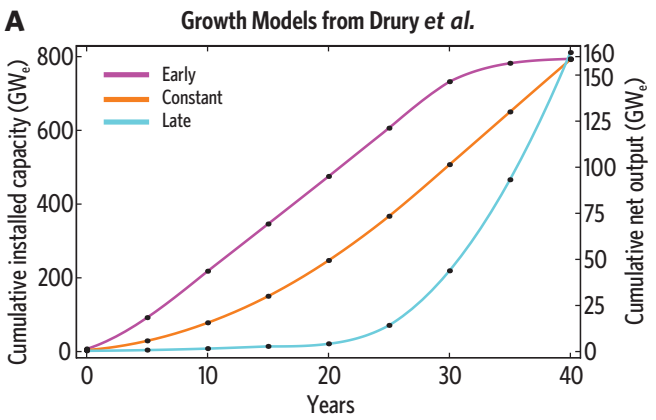

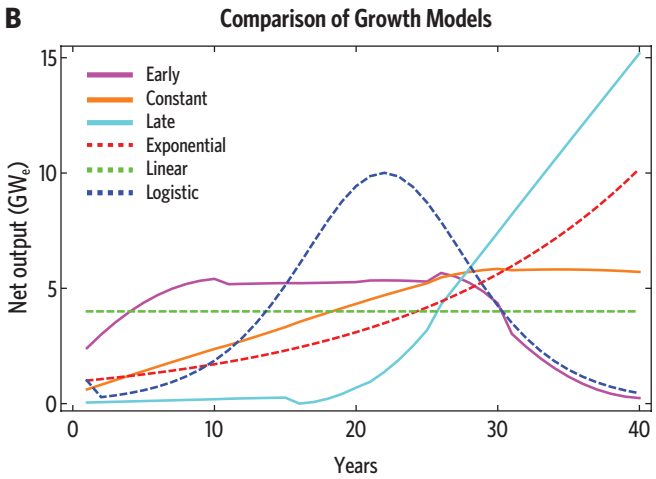

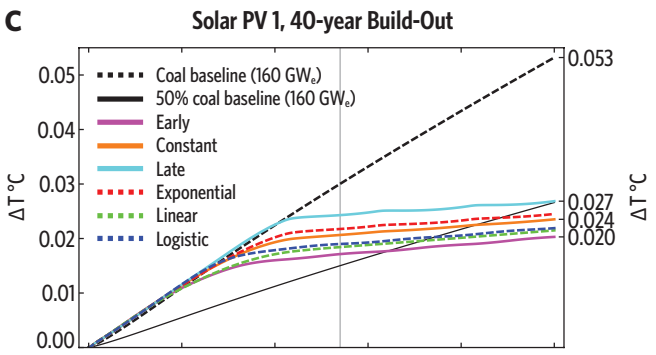

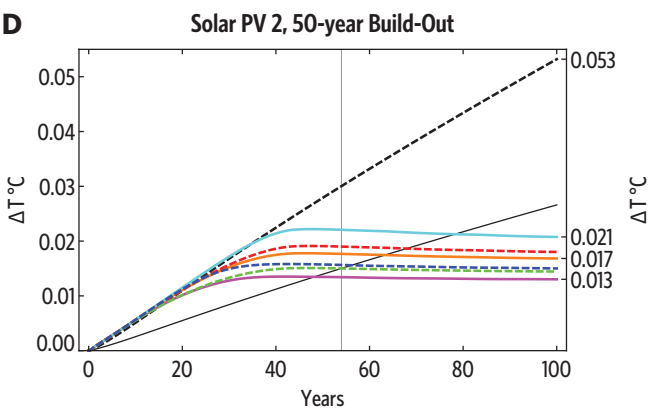

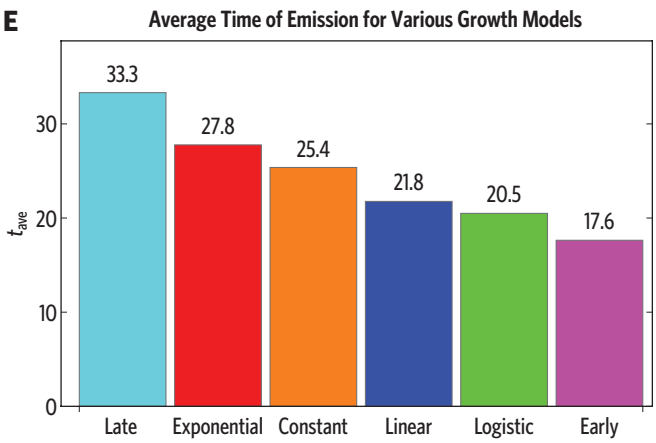
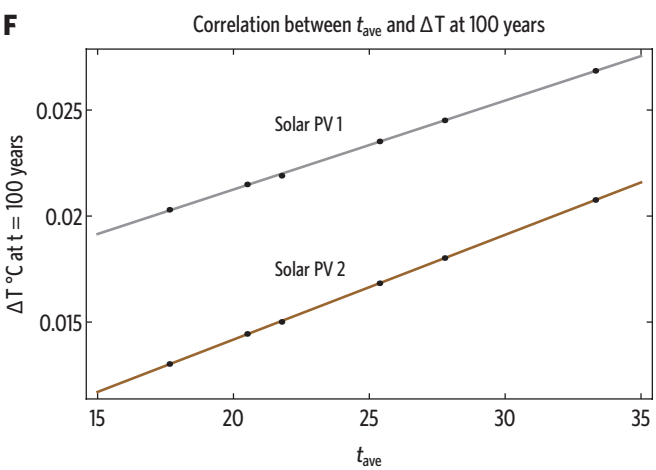
Figure S15. Results are shown for growth models from Drury *et al.* [45] (**A**) Three growth models for 40 y build-outs of 160 GW_e of net output of solar photovoltaic (PV) generation. Black points show data from tables in Drury *et al.*; curves are interpolated. (**B**) The additional output added each year for the Drury and team models based on the extrapolated curves as well as exponential, linear and logistic growth as developed in this paper. (**C**) ΔT for each growth curve obtained by using the emission data for Solar PV 1. (**D**) ΔT for each growth curve for Solar PV 2, which is approximately the same as the data set used in Drury *et al.* The black dashed line shows ΔT for coal producing a constant net output of 160 GW_e. The thin black line shows 50% ΔT for the same coal system; where this intersects the ΔT curves are the points at which the temperature increase is 50% of that produced by coal, which occurs at time $t_{0.5}$. The results from Drury *et al.* bracket the ΔT results for exponential, linear, and logistic growth curves; the late-transition curve is always above the exponential, the early-transition curve is always below the linear model, and the constant-transition curve is between the exponential and the logistic curves. Linear and logistic give very similar results for $t \geq 40$ years. (**E**) The average time of emission, t_{ave}, weighted by the annual emissions from (**B**). t_{ave} has the same ordering as ΔT in (**C**) or (**D**); the late transition ranks first, and the other transitions rank according to the appropriate order of ΔT sorted from high to low; the lowest average time of emissions results from the early transition, which also has the lowest ΔT. (**F**) The correlation between the ΔT and t_{ave} for simulations obtained by using data from the Solar PV 1 (gray line) and Solar PV 2 (brown line) cases. This figure shows that t_{ave} is an excellent predictor of long-term ΔT, with ($R^2 > 0.999$).